Recurring Lacustrine Depositional Successions in the Wilkins Peak Member, Green River Formation: The Basin-Center Evaporite Perspective

Elizabeth M. Klonowski[1], Tim K. Lowenstein[1], Alan R. Carroll[2], M. Elliot Smith[3], Matteo Paperini[4], and Jeffrey T. Pietras[1]

[1]*Department of Geological Sciences and Environmental Studies, Binghamton University, Binghamton, New York, eklonow1@binghamton.edu*
[2]*Department of Geoscience, University of Wisconsin-Madison, Madison, Wisconsin*
[3]*School of Earth Science and Environmental Sustainability, Northern Arizona University, Flagstaff, Arizona*
[4]*Mine Engineering Dept., Solvay Chemicals, Inc., Green River, Wyoming*

ABSTRACT

Mineralogy, petrographic textures, and sedimentary structures from the world's largest trona deposit, the Wilkins Peak Member (WPM) of the early Eocene Green River Formation (GRF), Bridger subbasin, Wyoming, provide key data about depositional conditions and paleoenvironments. The 250 m-long WPM interval in the Solvay S-34-1 drill core analyzed in this study contains a detailed record of sedimentation in the Bridger subbasin at the deepest area of a hydrologically-closed basin during peak Cenozoic atmospheric CO_2 concentrations. Large accumulations of trona ($Na_3(HCO_3)(CO_3)\cdot 2H_2O$), shortite ($Na_2Ca_2(CO_3)_3$), northupite ($Na_3Mg(CO_3)_2Cl$), and halite (NaCl; now replaced by trona), occur in the lower half of the WPM. Modern saline lake environments such as Lake Magadi, Kenya, and the Dead Sea, Israel-Jordan, are useful analogues for interpreting paleolake conditions associated with evaporite deposition in the Solvay S-34-1 core. Solvay saline lake deposits are organized into meter-scale shallowing-upward successions, beginning with (1) oil shale overlain by (2) trona, in places interbedded with oil shale, followed by (3) peloidal dolomite grainstone and/or silty dolomitic mudstone, and (4) massive mudstone with disruption features or desiccation cracks, and/or siliciclastic sandstone with ripple cross-stratification. Based on observations of modern hypersaline lake environments, WPM evaporite deposition at the basin depocenter is interpreted to be controlled by inflow water composition and volume, evaporative concentration, and seasonally-driven lake temperature fluctuations, resulting in recurrent patterns in evaporite mineralogies and textures.

INTRODUCTION

The Eocene Wilkins Peak Member (WPM) of the Green River Formation (GRF), Wyoming, consists of lacustrine strata that host the world's largest oil shale and sodium carbonate evaporite accumulations (Dyni, 1996; Johnson et al., 2010). The WPM was deposited in the Bridger Basin of the Greater Green River Basin (GGRB) from ~51.3-49.6 Ma (Smith et al., 2008, 2010).

Many studies have interpreted the paleoenvironments of WPM sedimentary rocks (Bradley and Eugster, 1969; Eugster and Hardie, 1975; Dyni, 1996; Dyni, 1998; Smoot, 1983. Pietras and Carroll, 2006; Jagniecki and Lowenstein, 2015; Smith et al., 2015), but the specific settings in which the evaporites were deposited have been debated. Previous outcrop-based studies (Eugster and Hardie, 1975; Smoot, 1983; Bohacs, 1998; Pietras and Carroll, 2006) interpreted the evaporite facies to represent periods when the paleolake dried out into a saline pan or mudflat. In contrast, based on subsurface investigation, Jagniecki and Lowenstein (2015) reinterpreted these deposits to have formed during deeper lake periods with perennial, at times, density stratified conditions, and hypersaline bottom waters. Modern perennial saline lakes are meters (Great Salt Lake) to hundreds of meters deep (Dead Sea) and contain brines that persist for tens to many thousands of years (Smoot and Lowenstein, 1991).

Meter-scale facies successions have long been recognized in the WPM and attributed to alternating episodes of lake expansion and contraction (Eugster and Hardie, 1975; Smoot, 1983; Fischer and Roberts, 1991; Pietras and Carroll, 2006; Aswasereelert et al., 2013; Jagniecki and Lowenstein, 2015; Smith et al., 2015). The driving mechanisms that produced the WPM lake stratal successions, however, are debated. Several studies have concluded that these successions reflect orbital forcing of sedimentation at Milankovitch-band frequencies (Fischer and Roberts, 1991; Meyers et al., 2008; Aswasereelert et al., 2013; Smith et al., 2014), although some WPM successions appear to be sub-precessional in duration and therefore may

result from other mechanisms such as geomorphic instability of the surrounding landscape (Pietras et al., 2003; Pietras and Carroll, 2006).

In 2016, Solvay Minerals drilled the 642 m-long Solvay S-34-1 core which contains a nearly complete record of GRF sedimentation in the Bridger subbasin near its hydrologic low point at the deepest area of the closed-basin (Figure 1). This study analyzed 250 m of the WPM in the Solvay S-34-1 core. Here, we (1) describe the WPM sedimentary rocks with emphasis on the evaporitic intervals, 2) compare WPM evaporite to modern analogs in order to interpret lake depths, chemistries, and depositional settings, and 3) apply these data to better constrain the paleoenvironmental evolution of the WPM shallowing-upward successions.

GEOLOGIC BACKGROUND AND PREVIOUS WORK

The GGRB was a broad, low relief basin bounded by the Cordilleran fold and thrust belt to the west and Laramide basement uplifts to the north, east and south (Figure 1) (Smith et al., 2015). Lake Gosiute occupied the Bridger, Great Divide, Washakie, and Sand Wash subbasins of the GGRB for ~4-5 myr in the Eocene and deposited the Tipton Member (~52.5-51.6 Ma), WPM (~51.6-49.9 Ma), and Laney Member (~49.9-48.5 Ma) in the Bridger subbasin (Smith et al., 2008; Smith et al., 2010; Smith et al., 2015) (Figure 2). The Bridger subbasin is generally free of structural complications with most rocks dipping less than 2°, aside from the Rock Springs uplift located along the eastern margin of the basin, and the Sevier fold-thrust belt that bounds the west edge of the basin (Eugster and Hardie, 1975) (Figure 2).

The WPM is up to 400 m thick in the Bridger subbasin (Dyni, 1996; Roehler, 1992). The WPM is thickest near the Uinta uplift and thins out completely before reaching the southern portion of the Wind River Mountains, Wyoming (Figure 1) (Pietras and Carroll, 2006; Smith et al., 2015). The WPM contains >127 billion tons of trona ($Na_3(HCO_3)(CO_3)\cdot 2H_2O$) and > 10,500 km^2 of disseminated shortite ($Na_2Ca_2(CO_3)_3$) (Dyni, 1996). There are as many as 40 sequentially numbered Trona Beds in the WPM that range in thickness from a few centimeters to about 12 m and 25 beds are > 1 m in thickness (Culbertson, 1966; Dyni, 1996). The term "Trona Bed" is used here to describe intervals that are predominantly composed of laminated to bedded trona, in places interlayered with dolomitic mudstone and organic-matter-rich dolomitic mudstone (oil shale). Due to a northward shift in the basin depocenter after deposition of Trona Bed 16, only eighteen of the 25 Trona Beds with a thickness > 1 m were deposited in the southern Bridger subbasin. These lower 18 Trona Beds contain trona and, in places, halite, whereas Trona Beds 19-25 consist primarily of trona (Culbertson, 1966, 1971; Leigh, 1991; Wiig et al., 1995). Other evaporite minerals in the WPM include shortite ($Na_2Ca_2(CO_3)_3$), northupite ($Na_3Mg(CO_3)_2Cl$), and nahcolite ($NaHCO_3$) (Fahey, 1962; Culbertson, 1971; Robb and Smith, 1976).

The lacustrine depositional environments interpreted in the WPM have typically included three subenvironments: 1) perennial saline lake, 2) perennial saline lake shoreline, and 3) lake-fringing saline mudflat (Eugster and Hardie, 1975; Pietras and Carroll, 2006; Jagniecki and Lowenstein, 2015; Smith et al., 2015).

The perennial saline lake subenvironment includes trona, halite, and displacive evaporite commonly interbedded with laminated organic-matter-rich dolomitic mudstone. Bedded trona occurs as trona blades or needles 0.2-5 mm-long (Jagniecki and Lowenstein, 2015; Smith et al., 2015). Displacive evaporite typically crosscuts dolomitic mudstone beds in the form of shortite rhombs, 2-8 mm in diameter and <10 cm thick fracture fills (Jagniecki and Lowenstein, 2015; Smith et al., 2015). Interbedded evaporite and oil shale are now thought to have formed in a density-stratified lake (Jagniecki and Lowenstein, 2015; Smith et al., 2015).

The perennial lake shoreline subenvironment contains carbonate conglomerate, grainstone, and stromatolitic mudstone. Symmetrical wave ripples, simple trace fossils, and sand-sized peloids are common (Eugster and Hardie, 1975; Pietras and Carroll, 2006; Scott and Smith, 2015; Smith et al., 2015).

The lake-fringing saline mudflat subenvironment is composed of carbonate siltstone and disrupted calcareous mudstone-siltstone subfacies. Both subfacies contain dolomitic micrite and calcareous silt-sized clasts. Calcareous mudstone commonly contains diagenetic evaporite pseudomorphs, principally shortite replacing gaylussite or pirssonite, indicating the former occurrence of brines (Eugster and Hardie, 1975; Pietras and Carroll, 2006; Smith et al., 2015).

The alluvial environment is characterized by river channel, floodplain, and sheet delta deposits. The river channel and sheet delta subenvironments contain erosional scours and climbing cross-stratified-, trough cross-stratified-, planar-, and ripple-laminated-sandstone deposited by unidirectional current flow (Eugster and Hardie, 1975; Smoot and Lowenstein, 1991; Pietras and Carroll, 2006; Smith et al., 2015). Pebble-size intraclasts of mudstone, sandstone, and plant fragments record periods of high flow velocity, whereas mud drapes on rippled bedforms are indica-

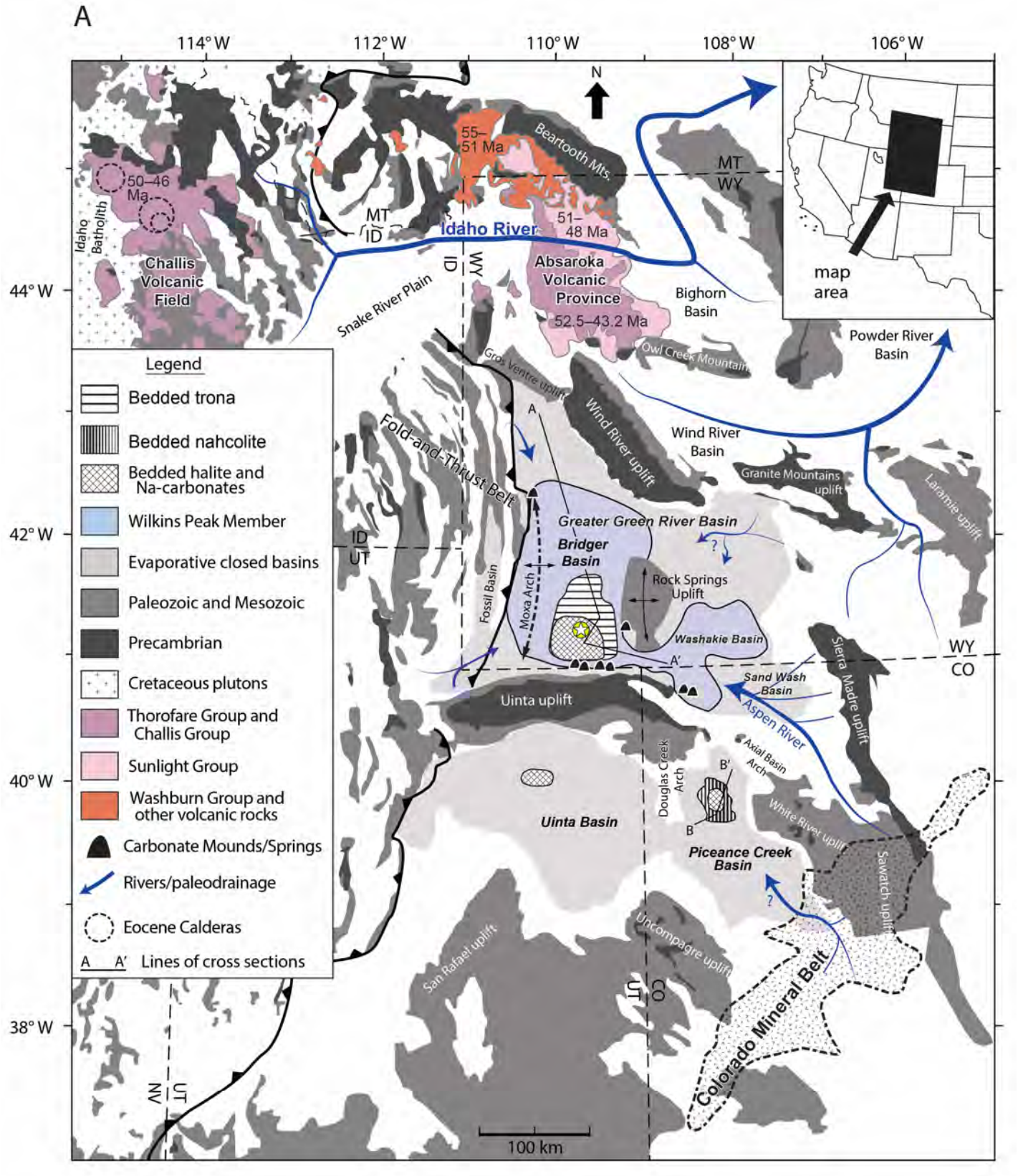

Figure 1. *General geologic map of Eocene basins and associated uplifts. White star inside yellow circle marks location of Solvay-S-34-1 core. (Adapted from Lowenstein et al., 2017).*

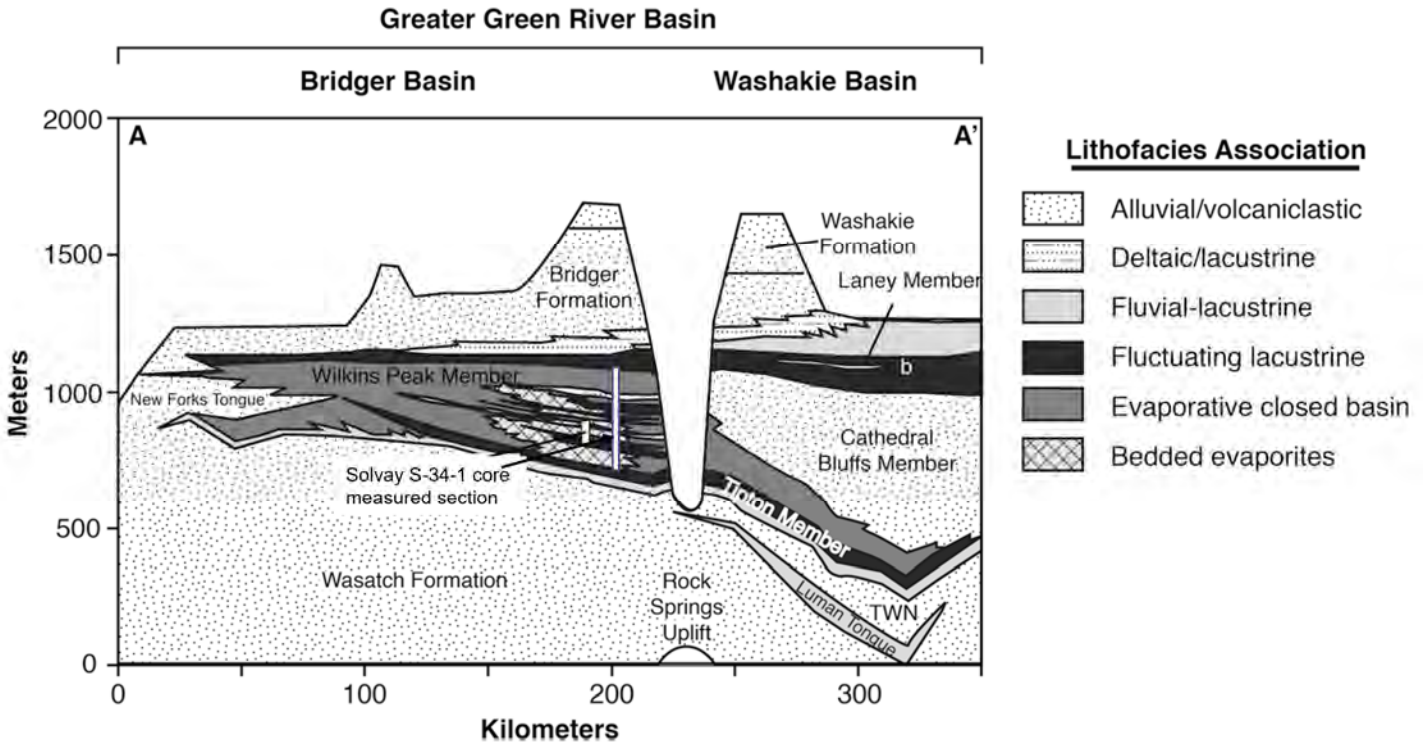

Figure 2. *Simplified cross section of the Bridger and Washakie Subbasins, Wyoming, through A—A' transect of Figure 1 with approximate location of the Solvay S-34-1 core. (Adapted from Jagniecki and Lowenstein, 2015).*

tive of slower currents (Pietras and Carroll, 2006; Smith et al., 2015).

The floodplain subenvironment is distinguished by massive (massive here meaning structureless mudstone with disruption features) to faintly-bedded green to brown siltstone and mudstone, with trace fossils, desiccation cracks, and incipient paleosols (Smoot, 1983; Pietras and Carroll, 2006; Smith et al., 2015).

The alluvial facies association in the WPM corresponds to the nine sandstone-siltstone-mudstone marker beds (A through I) originally described by Culbertson (1961). These alluvial marker beds (up to 25 m thick) are correlated across the Bridger subbasin (Culbertson, 1961; Smoot, 1983; Pietras and Carroll, 2006; Smith et al., 2008, 2015).

The WPM is well-known for the many shallowing -upward successions that occur on the meter-scale (Eugster and Hardie, 1975). Smoot (1983) described such WPM successions as alternations between shallow, marginal lake and deeper perennial lake deposits. Pietras and Carroll (2006) and Smith et al. (2015) described WPM basin expansion-contraction cycles as repetitive facies successions beginning with transgressive deposits, followed by deep-lake oil shale and detrital carbonate, and capped with disrupted mudstone, siltstone, and evaporite.

Although the WPM facies successions are well recognized and documented, less work has been done detailing the evaporitic component of these successions. The evaporites in the Solvay S-34-1 core exhibit sedimentary structures which suggest they were deposited subaqueously, not in exposed saline pans as interpreted by previous workers (Eugster and Hardie, 1975; Smoot, 1983; Pietras and Carroll, 2006; Smith et al., 2015). Here, we describe the evaporites in the lower WPM in the Solvay S-34-1 core and interpret the environments in which they were deposited, which provides new details about the recurring successions in the GRF.

METHODS

The Solvay S-34-1 NQ-diameter (47.6 mm) core was drilled in southwestern Wyoming by Solvay Minerals in 2016. This core was taken near the hydrologic low-point of the Bridger subbasin (Figure 1), and includes ~250 meters of the WPM that contains Trona Beds 1-18. The uppermost WPM is not represented due to a facies change to sandstone. Two hundred samples were collected at ~30 cm intervals for petrographic and mineralogical analysis at the National Lacustrine Core Facility (LacCore), University of Minnesota, for the entire WPM interval. The WPM of the Solvay S-34-1 core was described for its lithology and sedimentological features at the ~1 cm scale (Figure 3).

Forty-seven 5 cm x 7 cm thin sections of various

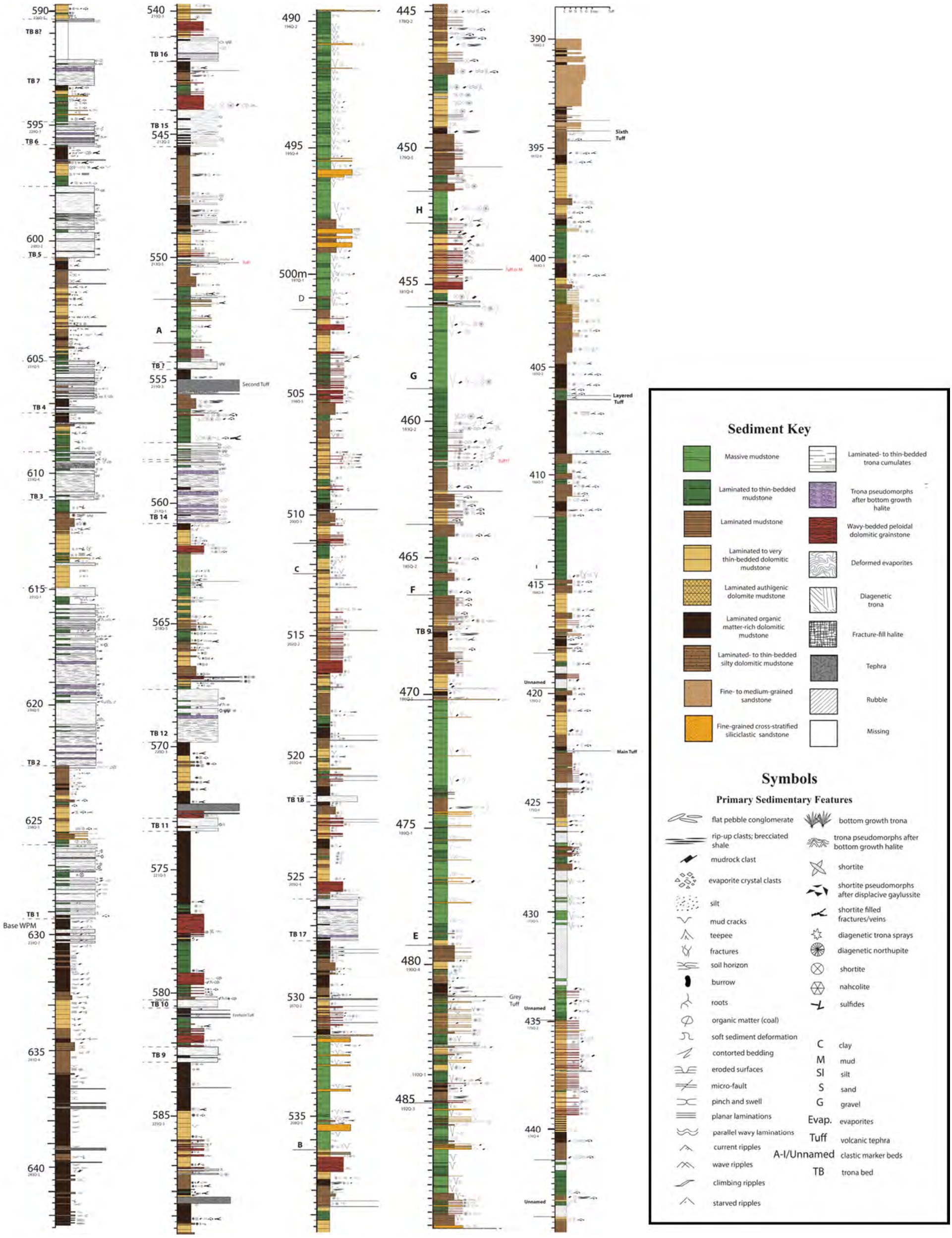

Figure 3. *Measured section and lithologic key, 390-642 mbs of Solvay S-34-1, Wilkins Peak Member. Section shows bottom (left) to top (right).*

WPM lithologies were made for transmitted light microscopy on a Zeiss Axio Imager.A1, and a Leica Wild-M3Z, with a Nikon Plan APO 1.0x objective. Samples were examined to distinguish depositional textures and primary versus secondary evaporite mineralogy.

Mineralogical characterization of 86 samples from the Solvay S-34-1 core was performed using X-ray diffraction (XRD). A handheld Dremel tool was used to sample laminae as thin as 2 mm-thickness. Powdered samples were analyzed using a Philips Xpert PW3040-MPD diffractometer operated at 40 kV and 20 mA, using Cu-Kα radiation fitted with a diffracted-beam graphite monochromator. Continuous scans were run from 10.00° to 50.0° 2θ with step sizes of 0.030° at 0.80 seconds per step. Minerals were identified by comparing the dominant peaks to known patterns in the "High Score Plus" mineral database.

A Field Emission Scanning Electron Microscope (SEM) Zeiss Supra 55 VP was used to study ten samples and distinguish between detrital and authigenic carbonate mud. Rock chips were coated with carbon using the arc discharge method for SEM-EDX and mounted on a sputter coated gold plate. Coated samples were analyzed at 3 kV to 10 kV under vacuum with back scattered electrons (BSE) and secondary electrons (SE).

Measured sections of the WPM were constructed from core observations and from images of the cores. Thin sections clarified grain relationships and diagenetic features. Macroscopic and microscopic features were plotted on the measured sections at the depths of observation.

WPM FACIES AND DEPOSITIONAL ENVIRONMENTS

Facies observed in the WPM interval of the Solvay S-34-1 core are interpreted to have been deposited in two predominant depositional environments: (1) perennial saline lake and (2) alluvial mudflat/sheet delta (Culbertson, 1962; Eugster and Hardie, 1975; Pietras and Carroll, 2006; Jagniecki and Lowenstein, 2015; Smith et al., 2015).

Perennial Saline Lake Facies

The evaporite subfacies in the Solvay S-34-1 core includes: 1) laminated to bedded trona cumulates, 2) radiating vertically-oriented trona and 3) trona pseudomorphs after vertically-oriented halite. Trona and dolomite occur as primary and diagenetic minerals, whereas shortite and northupite are strictly diagenetic minerals. The mudstone subfacies contains: 1) organic-matter-rich dolomitic mudstone (oil shale), 2) authigenic dolomite mudstone (rare), and 3) laminated-thin bedded dolomitic (silty) mudstone. Coarser, wavy bedded carbonates form the peloidal dolomite grainstone subfacies.

Evaporite Subfacies

Trona Cumulates

Description: Trona is the major sodium carbonate mineral in the WPM in the Bridger subbasin. The most common texture in Trona Beds 1-18 is microcrystalline cumulate that occurs in laminae, ~1 mm to 1 cm thick (Figure 4a). Trona cumulates are composed of well-sorted trona needles, 50-200 μm long, arranged with their longest axis subparallel to bedding (Figure 4b, c). Cumulate trona is commonly interbedded with laminated organic-matter-rich dolomitic mudstone (oil shale).

Interpretation: The alignment and well-sorted nature of trona crystals indicates a primary "settle out" origin, whereby trona precipitated in the water column and crystals fell out of suspension (Leigh, 1991; Boni and Atkinson, 1998). Lack of dissolution suggests trona cumulates were deposited in a density stratified lake in which crystals on the basin floor were protected from fresh water inflow by dense saline bottom brines (Jagniecki and Lowenstein, 2015). The interlayering of trona with oil shale suggests accumulation in an anoxic, alkaline, saline lake (Figure 4a) (Boni and Atkinson, 1998; Jagniecki and Lowenstein, 2015).

Cumulate layers composed of halite from the modern Dead Sea, although different in mineralogy, exhibit similar textures to the WPM trona cumulates in the Solvay S-34-1 core. In the Dead Sea, halite cumulates form when lake waters cool from ~35º C to ~24º C during the winter months (Sirota et al., 2017). Because halite solubility is greatest at elevated temperatures, winter cooling results in supersaturation and precipitation of fine, cumulate halite crystals in the water column (Figure 5). If halite cumulates are deposited below the thermocline (> ~20-30 m depth in the modern Dead Sea), they are protected from subsequent dissolution by dilute flood waters and warm, undersaturated summer lake waters. The conditions under which halite is deposited and preserved in the Dead Sea today (Sirota et al., 2017) suggest that trona, also with greater solubility as brine temperatures increase, was deposited during the colder, winter months, below the thermocline of Lake Gosiute (Demicco and Lowenstein, 2020; Olson and Lowenstein, 2021).

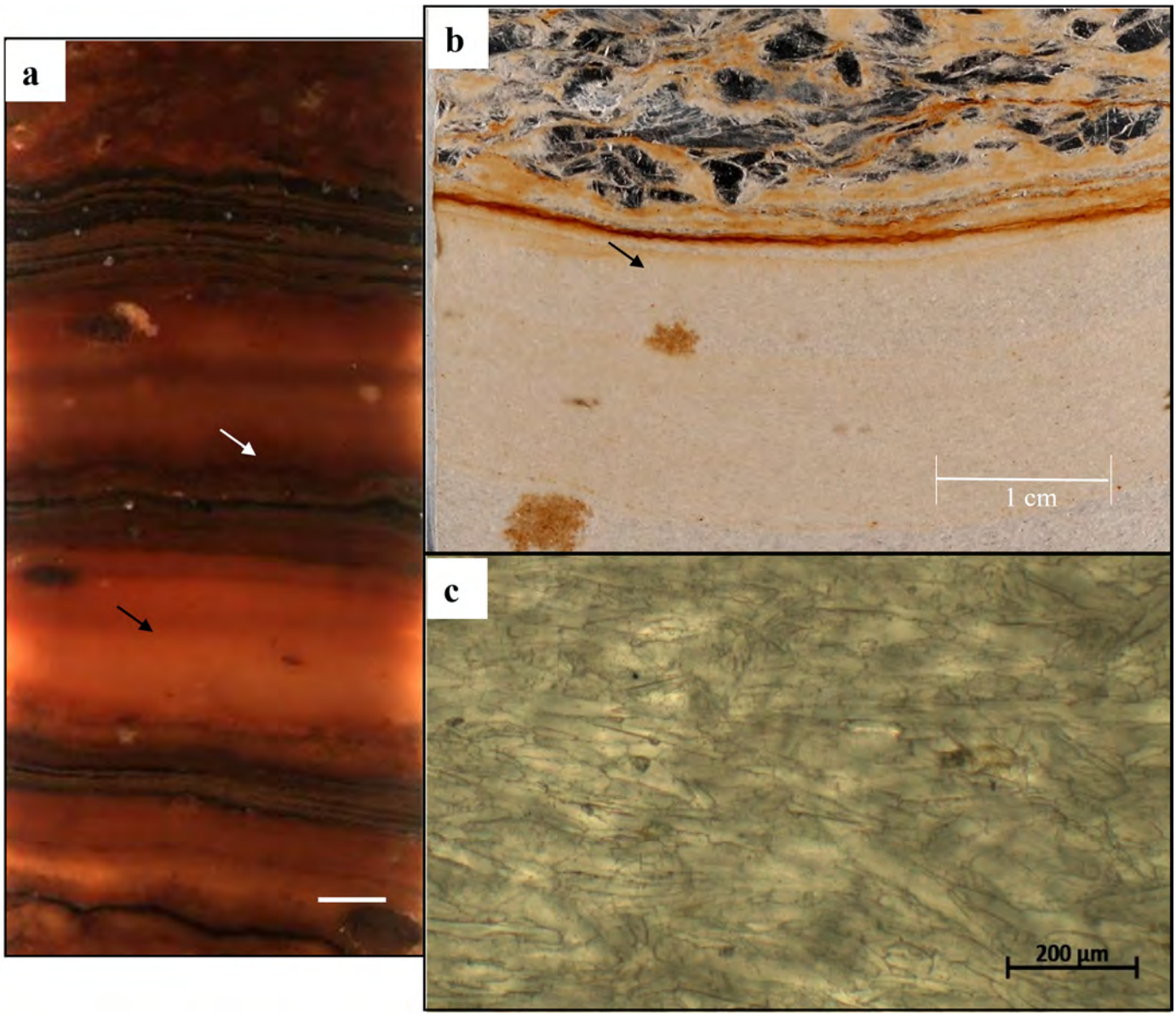

Figure 4. *a) Core photograph of cumulate trona laminae (black arrow) interlayered with oil shale (white arrow). GRCO-GRF16-1A-217Q-2-W (560.12-560.75 mbs). Scale bar = 1 cm. Thin section photographs of b) Cumulate trona laminae (black arrow to base of photo). GRCO-GRF16-1A-206Q-2-W (526.68-527.15 mbs). c) Well sorted cumulate trona crystals oriented parallel to bedding. GRCO-GRF16-1A-206Q-2-W (526.68-527.15 mbs).*

Radiating Vertically Oriented Evaporite (Bottom-Growth Evaporite)

Description: In the Solvay S-34-1 core, there are ~20 occurrences of radiating vertically oriented, competitively-grown, trona crystals ~2 mm to 5 cm in length, within trona cumulate beds (Figure 6 a,b). These crystal textures represent < 10 % of the total trona in the Solvay S-34-1 core. Overlying trona cumulates thicken between vertically oriented crystals and thin at their tops. Rarely (4 occurrences in Trona Beds 5, 12, 17, and unnamed Trona Bed at 554.5 m), vertically oriented trona layers contain horizontal dissolution surfaces (Figure 6b) (Smoot, 1983; Lowenstein and Hardie, 1985; Jagniecki and Lowenstein, 2015).

In the Solvay S-34-1 core, trona commonly occurs as a pseudomorphous replacement of euhedral halite crystals with vertical, upward growth fabrics (Figure 5). The trona crystals replacing halite are ~ 200 µm to 5 mm in length. It is rare to find well-preserved primary halite that has not been partially or completely replaced by trona in the Solvay S-34-1 core. The pseudomorphs are draped by microcrystalline trona cumulates.

Interpretation: Bottom growth trona and halite crusts precipitated from bottom brines in a density stratified saline lake (Jagniecki and Lowenstein, 2015). Bottom growth halite forms year-round in the modern Dead Sea, where, if crystallized below the thermocline, it is protected from dissolution due to

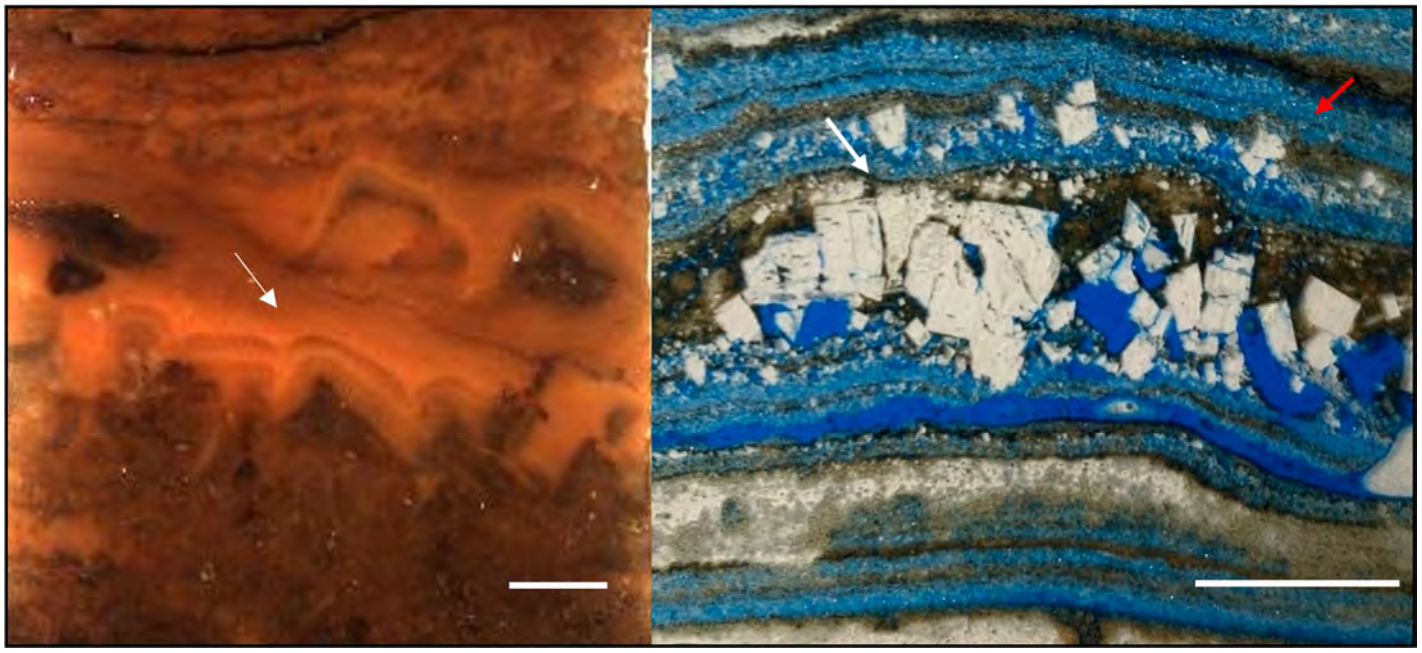

Figure 5. *Left: Trona pseudomorphs after bottom growth halite (white arrow). Well preserved halite crystal structure and trona cumulate drapes above the pseudomorphs indicate deposition below the thermocline of a deep lake (> ~20 m). Core image from GRCO-GRF16-1A-217Q-3-W (560.83-561.75 mbs) Right: Thin section photograph of well-preserved, coarse bottom growth halite (white arrow) and cumulate halite (red arrow) from the modern Dead Sea shoreline, deposited when lake depths were ~30 m. Blue color is epoxy-filled pore space. Bottom-growth halite forms year-round, whereas cumulate halite is deposited only in winter months (Sirota et al., 2018). Scale bar = 1 cm for both images.*

seasonal variations in lake water temperature and dilute floodwaters entering the basin (Sirota et al., 2017). These observations and the general absence of synsedimentary dissolution features in bottom growth halite pseudomorphs of the WPM suggests that the halite formed below the thermocline of a density stratified hypersaline lake (Smoot and Lowenstein, 1991; Lowenstein et al., 1999; Sirota et al., 2017).

Bottom growth trona with dissolution surfaces is similar in appearance to the bottom growth trona from modern Lake Magadi, Kenya (Figure 6b,c) (McNulty et al., 2017). There, trona crusts develop on the bottom of a shallow hypersaline lake < 1 m deep that commonly dries out. When dilute floodwaters enter the Magadi Basin, the trona partially to completely dissolves (Figure 6c). This suggests that bottom growth trona with dissolution surfaces in the Solvay core was deposited in a shallow saline lake which did not protect trona crystals at the sediment-brine interface from dissolving when dilute flood waters reached the basin depocenter.

Our observations suggest that most WPM evaporite was deposited below the thermocline, with rare deposition above the thermocline. The thermocline of the modern Dead Sea is 20-30 m below the lake surface. While this depth range cannot be precisely applied to the Eocene due to uncertainty in environmental factors such as climate, salinity, and lake hypsometry, it is a useful rough analogy for minimum depth of evaporite accumulation in ancient Lake Gosiute.

Mudstone Subfacies

Organic-Matter-Rich Dolomitic Mudstone (Oil Shale)

Description: Organic-matter-rich dolomitic mudstone (oil shale) is mm-scale laminated (0.5 to 5 mm), dolomite-rich with minor quartz, and honey brown to black color (Table 1; Figure 7a,b). Laminae are planar to wavy with soft sediment deformation features such as loop bedding and convolute bedding. Highly compacted, matrix-supported oil shale breccias are commonly associated with oil shale (Figure 7c) (Dyni and Hawkins, 1981). The organic matter in oil shale (up to 19% total organic carbon) is derived from algae and bacteria (Bradley, 1962; Tissot and Vandenbroucke, 1983; Bohacs, 1998; Carroll and Bohacs, 2001; Pietras et al., 2006). Trona is commonly interbedded with oil shale. Sulfide minerals, such as pyrite, are rare. Diagenetic fracture-fill shortite and nodular northupite are common in this lithology.

Interpretation: The preservation of organic matter, sulfide minerals, and sodium carbonate evaporites, and the lack of bioturbation, suggest that these mudstones were originally deposited in an anoxic alkaline Na-CO_3-rich perennial saline lake similar in chemical composition and depth (> 10 m) to modern Mono Lake, California, USA and Lake Bogoria, Kenya (Domagalski et al., 1989; Renaut et al., 2013).

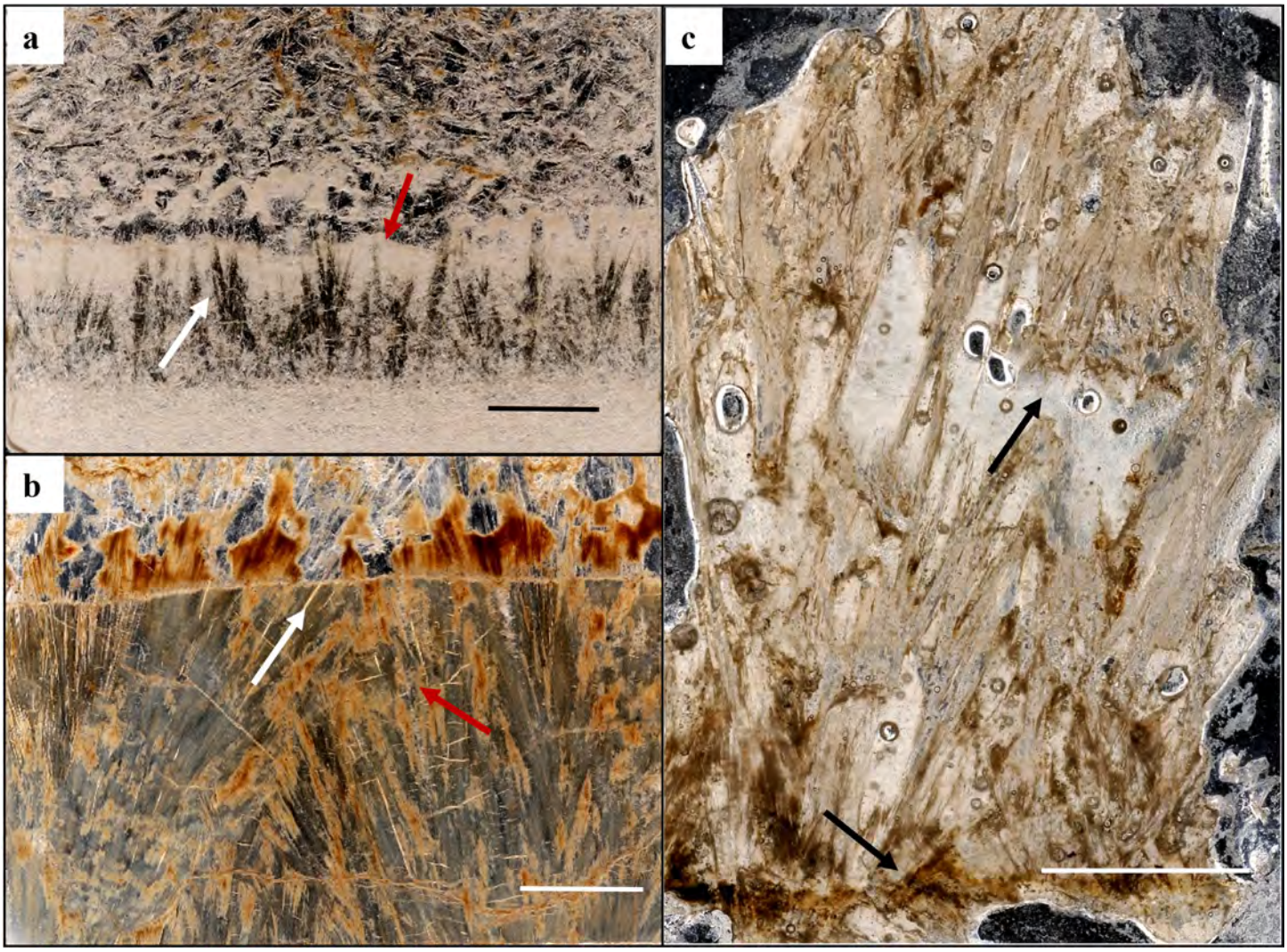

Figure 6. *Thin section photographs of: a) Bottom growth trona (white arrow) overlain by cumulate trona drapes (red arrow). Bottom growth trona lacks dissolution surface suggesting deposition below the thermocline. GRCO-GRF16-1A-230Q-3-W (600.44-601.07 mbs). b) Bottom growth trona needles with competitive growth (red arrow) and dissolution surface (white arrow) suggesting deposition above the thermocline. GRCO-GRF16-1A-230Q-2-W (599.83-600.44 mbs). c) Bottom growth trona from subsurface core, Lake Magadi, Kenya HSPDP-MAG14-2A-4Y-1 (~10 mbs). Black arrows show dissolution surfaces. Scale bar = 1 cm on all images.*

Authigenic Dolomite Mudstone

Description: Laminated (0.1-1 cm) authigenic dolomite mudstone is pale yellow-brown to white in color and relatively rare in the Solvay core (~40 thin beds are noted in the detailed measured section) (Figure 7d). Dolomite laminae are virtually monominerallic and lack diagenetic evaporite and sulfides. X-ray diffraction analyses conducted on authigenic dolomite mudstone showed that feldspars and mica are absent, and quartz is sparse (Figure 8a). SEM analysis showed that this mudstone is composed of well-sorted 5 to 10 µm dolomite crystals. Dolomite laminae are commonly grouped into 1 to 3 cm thick packages that exhibit soft sediment deformation and compaction structures. Authigenic dolomite mudstone packages are interlayered with oil shale and laminated - to thin-bedded dolomitic mudstone (Figure 7d).

Interpretation: Murphy et al. (2014) interpreted carbonate mudstone in the WPM and Laney Member as authigenic on the basis of homogeneous laminae composed of well-sorted crystals, carbonate crystal size of < 10 µm, and preservation of primary pore space (Murphy et al., 2014). Authigenic dolomite laminae in the Solvay S-34-1 core exhibit similar features.

Laminated-Very Thin-Bedded Dolomitic (Silty) Mudstone (Silty Dolomitic Mudstone)

Description: Laminated to very thin-bedded (1-2 cm thick) dolomitic mudstone, with clay- to silt-sized grains, ranges from brown to green to dull yellow in color (Figure 7d, e, f, g). Layers are commonly composed of dolomite, potassium feldspar, quartz, muscovite and biotite (Table 1) (Figure 8b). Silty dolomitic

Table 1: *Composite XRD Data from 86 samples of varying lithologies in the Solvay S-34-1 core. Lithology key: Oil shale (OS); Laminated to thin-bedded detrital mudstone (MS); Carbonate mudstone (CMS); Laminated to thin-bedded silty mudstone (SMS); Wavy-bedded peloidal grainstone (WBP); Evaporites (EVAP); Tuff (TUFF).*

Drive (SRCD-SRF-16-1A)	Sample Depth Top (cm)	Sample Depth Bottom (cm)	Top Depth (ft)	Bottom Depth (ft)	Top Depth (mbs)	Bottom Depth	Quartz	Trona	Halite	Northupite	Shortite	Nahcolite	Enstatite	Calcite	Dolomite	Orthoclase	Paligioclase Feldspar	Glauconite	Muscovite	Magnetite	Pyrite	Pyrrhotite	Lithology
168Q-5	25.5	28.5	1363.9	1365.9	415.7	416.3																	CMS
175Q-4	8	12	1432.4	1434.5	436.6	437.2																	CMS
175Q-5	35	39	1434.5	1436.6	437.2	437.9																	WBP
175Q-6	28	32	1436.6	1437.7	437.9	438.2																	WBP
178Q-4	8	12	1463	1465.1	445.9	446.5																	CMS
181Q-2	11	15	1488.3	1490.3	453.6	454.3																	WBP
191Q-2	18	22	1579	1581.1	481.3	481.9																	CMS
191Q-3	7	11	1581.1	1583	481.9	482.5																	CMS
191Q-4	28.5	32.5	1583	1585	482.5	483.1																	CMS
198Q-4	14.5	18.5	1652.7	1654.7	503.7	504.4																	WBP
198Q-4	58.5	62.5	1652.7	1654.7	503.7	504.4																	WBP
204Q-2	53	57	1707.4	1709.4	520.4	521																	CMS
204Q-5	33.5	37.5	1713.4	1715.4	522.3	522.9																	MS
204Q-6	29	33	1715.4	1716.9	522.9	523.3																	MS
205Q-2	43.5	47.5	1717.4	1719.3	523.5	524.1																	MS
205Q-3	55	59	1719.3	1721.4	524.1	524.7																	MS+EVAP
205Q-5	23	27	1723.4	1725.4	525.3	525.9																	MS
205Q-6	28.5	32.5	1725.4	1727.1	525.9	526.4																	MS+EVAP
206Q-1	0	4	1727	1728	526.4	526.7																	EVAP
206Q-1	0	4	1727	1728	526.4	526.7																	MS+EVAP
206Q-2	5	9	1728	1729.5	526.7	527.1																	EVAP
206Q-2	5	9	1728	1729.5	526.7	527.1																	MS+EVAP
206Q-2	30	34	1728	1729.5	526.7	527.1																	EVAP
206Q-3	20	24	1729.5	1731.3	527.1	527.7																	EVAP
206Q-3	20	24	1729.5	1731.3	527.1	527.7																	EVAP
207Q-1	11	15	1737	1737.1	529.4	529.5																	OS
207Q-1	39	43	1737	1737.1	529.4	529.5																	OS
207Q-2	52	56	1737.1	1739.1	529.5	530.1																	MS+EVAP
207Q-3	5	9	1739.1	1741.1	530.1	530.7																	MS+EVAP
208Q-4	0	4	1753	1755	534.3	534.9																	MS
208Q-4	55	57	1753	1755	534.3	534.9																	MS
208Q-5	38	42	1755	1757	534.9	535.5																	MS
208Q-6	0	3	1757	1757.1	535.5	535.6																	MS
209Q-1	18	22	1757	1758.8	535.5	536.1																	MS
209Q-2	52	56	1758.8	1760.8	536.1	536.7																	MS
209Q-3	5	7	1760.8	1762.8	536.7	537.3																	WBP
209Q-3	15	19	1760.8	1762.8	536.7	537.3																	MS+WBP
209Q-3	15	19	1760.8	1762.8	536.7	537.3																	MS+WBP
209Q-6	4	8	1766.9	1767.4	538.5	538.7																	MS
210Q-2	30.5	34.5	1768.4	1770.5	539	539.6																	MS
210Q-3	26	30	1770.5	1772.5	539.6	540.2																	MS
210Q-3	26	30	1770.5	1772.5	539.6	540.2																	MS+EVAP
210Q-4	5	9	1772.5	1774.5	540.3	540.9																	WBP
210Q-4	39	45	1772.5	1774.5	540.3	540.9																	EVAP
210Q-4	55	59	1772.5	1774.5	540.3	540.9																	EVAP
210Q-5	31	35	1774.5	1776.3	540.9	541.4																	MS+EVAP
210Q-5	31	35	1774.5	1776.3	540.9	541.4																	EVAP
211Q-3	51	55	1780.1	1782.1	542.6	543.2																	EVAP
211Q-3	51	55	1780.1	1782.1	542.6	543.2																	MS+EVAP
211Q-4	44	48	1782	1784	543.2	543.8																	WBP
211Q-4	5.5	9.5	1782	1784	543.2	543.8																	WBP
211Q-4	5.5	9.5	1782	1784	543.2	543.8																	EVAP
211Q-6	38	42	1785.9	1787.4	544.3	544.8																	MS
212Q-2	2	6	1787.4	1789.4	544.8	545.4																	EVAP
212Q-3	8	12	1789.4	1791.3	545.4	546																	CMS
212Q-4	43	47	1791.5	1793.4	546	546.6																	MS
212Q-5	11	15	1793.4	1795.4	546.6	547.2																	OS
212Q-5	42	46	1793.4	1795.4	546.6	547.2																	OS
213Q-5	10	14	1803	1804.9	549.6	550.1																	WBP
214Q-1	49	53	1807	1809	550.8	551.4																	SMS
214Q-5	5	9	1815	1817.1	553.2	553.8																	MS
214Q-5	57	61	1815	1817.1	553.2	553.8																	MS
214Q-5	57	61	1815	1817.1	553.2	553.8																	MS+EVAP
215Q-1	8	12	1817	1818.7	553.8	554.3																	WBP
215Q-4	22	26	1822.4	1824.4	555.5	556.1																	MS
215Q-5	36.5	37.5	1824.4	1826.4	556.1	556.7																	MS
216Q-6	26	30	1835.5	1836.7	559.5	559.8																	EVAP
217Q-4	23.5	27.5	1842	1844	561.4	562.1																	WBP
217Q-4	23.5	27.5	1842	1844	561.4	562.1																	EVAP
217Q-4	23.5	27.5	1842	1844	561.4	562.1																	WBP
218Q-4	44	48	1852.9	1854.6	564.8	565.3																	CMS
219Q-1	11	15	1857	1857.8	566	566.3																	CMS
219Q-4	6	8	1861.9	1863.9	567.5	568.1																	TUFF
219Q-4	18	22	1862	1864	567.5	568.1																	CMS
220Q-4	27	31	1871.4	1873.4	570.4	571																	MS+EVAP
222Q-4	46.5	50.5	1892.9	1895	577	577.6																	WBP
223Q-1	6	10	1897	1898.9	578.2	578.8																	EVAP
223Q-2	44	48	1898.9	1900.9	578.8	579.4																	MS
223Q-4	46.5	50.5	1902.9	1905	580	580.6																	EVAP
224Q-2	45	49	1908.7	1910.7	581.8	582.4																	WBP
231Q-6	6.5	10.5	1985.9	1987	605.3	605.6																	CMS
232Q-1	13	17	1987	1987.8	605.6	605.9																	CMS
232Q-2	0	4	1987.75	1989.8	605.9	606.5																	MS
234Q-1	42	44	2007	2008.7	611.7	664.7																	MS
236Q-1	22	32	2027	2028	617.8	618.1																	EVAP
238Q-4	49	53	2051.5	2053.4	625.3	625.9																	MS

mudstone contains rare sulfide minerals (pyrrhotite, pyrite, and marcasite), and abundant diagenetic shortite, some as a pseudomorphous replacement of gaylussite ($Na_2Ca(CO_3)_2 \cdot 5H_2O$) or pirssonite ($Na_2Ca(CO_3)_2 \cdot 2H_2O$) that grew displacively in brine saturated silty muds. Shortite also fills fractures.

Interpretation: Silt grains (Figure 7g) suggest lower lake levels that allowed transport of suspended siliciclastic sediment to the basin center from fluvial systems. The lack of disruption by burrowing or desiccation supports the hypothesis that these silty muds accumulated in a perennial lake, shallower and/or

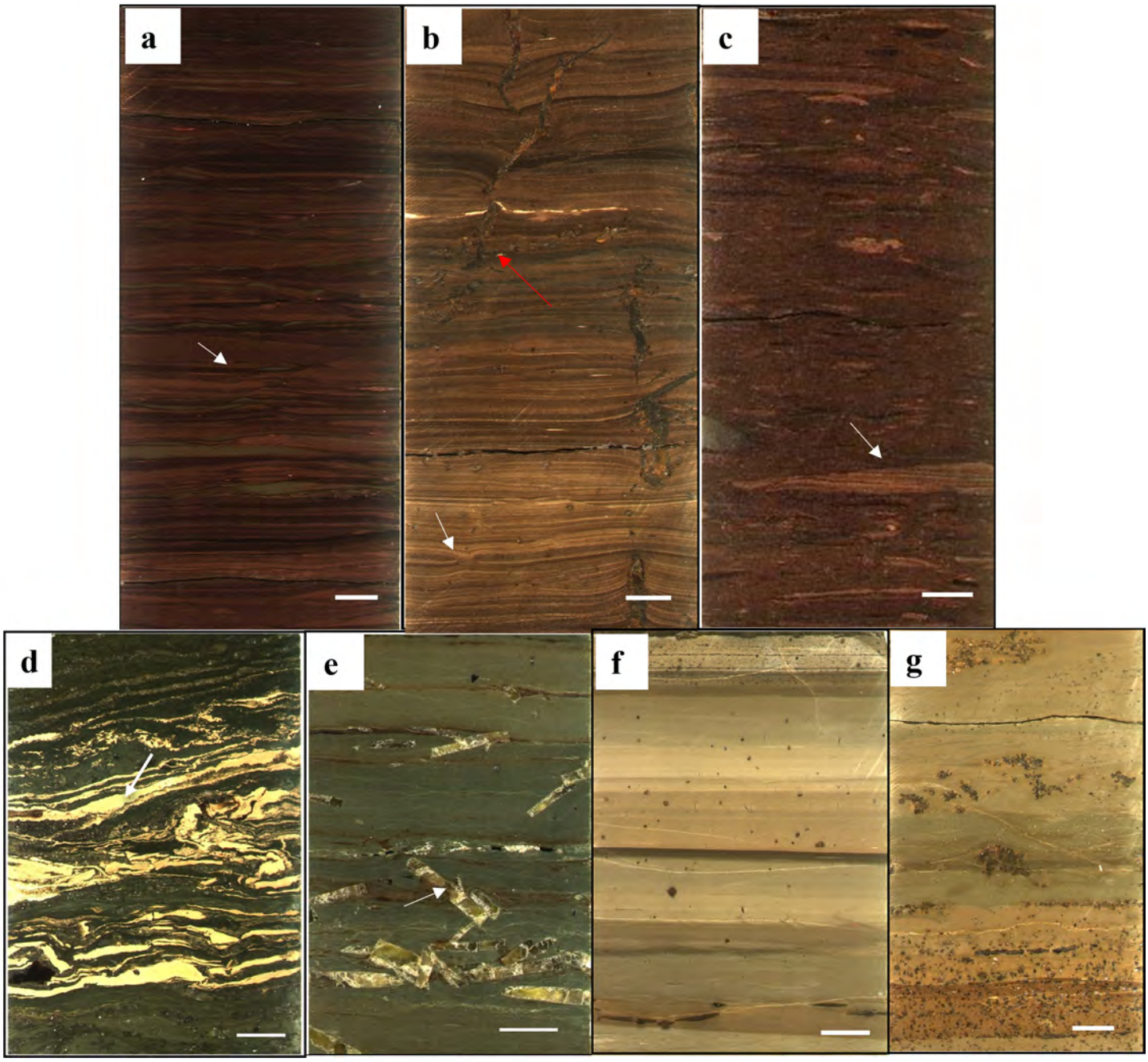

Figure 7. *Core photographs of: a) Organic-matter-rich dolomitic mudstone (oil shale), with compacted mud clasts (white arrow). GRCO-GRF16-1A-240Q-4-W (631.78-632.36 mbs). b) Oil shale with loop bedding (white arrow). Disruption feature is a displacive fracture filled with shortite (red arrow). GRCO-GRF16-1A-230Q-5-W (601.68-602.29 mbs). c) Oil shale breccia with large dolomitic mudstone clast (white arrow). GRCO-GRF16-1A-240Q-2-W (630.54-631.17 mbs). d) Authigenic dolomite mudstone (white arrow) with soft sediment deformation and interlaminated silty dolomitic mudstone. GRCO-GRF16-1A-217Q-6-W (562.65-563.17 mbs). e) Laminated- to very thin-bedded dolomitic mudstone with diagenetic shortite pseudomorphs after displacive gaylussite or pirssonite (white arrow). GRCO-GRF16-1A-233Q-3-W (609.37-609.99 mbs). f) Laminated- to very thin-bedded silty dolomitic mudstone. Silicate minerals associated with a detrital origin (quartz and muscovite) appear in XRD analysis. GRCO-GRF16-1A-226Q-5-W (589.94-590.53 mbs). g) Laminated- to very thin-bedded silty dolomitic mudstone with diagenetic shortite crystals. GRCO-GRF16-1A-199Q-2-W (505.44-506.06 mbs). Scale bar = 1 cm for all images.*

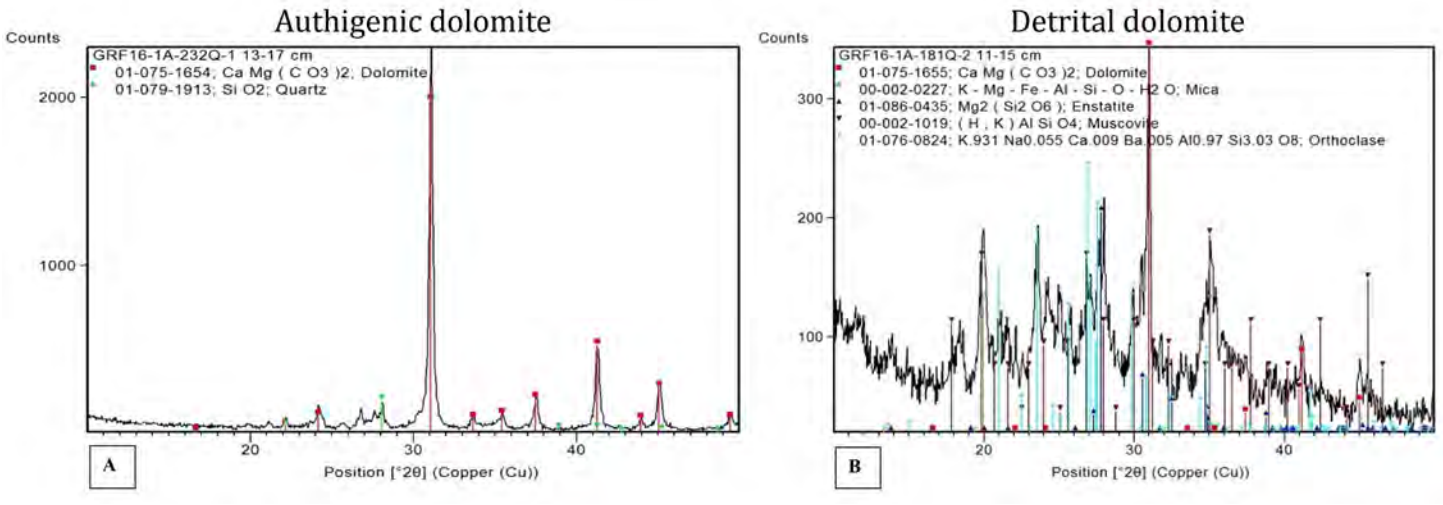

Figure 8. *X-Ray Diffraction scan of: a) Relatively pure dolomite composition confirms the authigenic origin of this mudstone. GRCO-GRF16-1A-232Q-1 13-17 cm (605.63-605.87 mbs). b) Occurrence of muscovite and orthoclase support detrital origin. GRCO-GRF16-1A-181Q-2 11-15 cm (453.64-454.25 mbs).*

closer to the shoreline than where oil shale was deposited. The lack of mudcracks suggests perennial lake conditions. Abundant diagenetic crystals of shortite, some pseudomorphous after gaylussite, are similar to those in Pleistocene Searles Lake, California, and indicate syndepositional brines (Figure 7e, g, 9) (Olson and Lowenstein, 2021). At Searles Lake, gaylussite formed by replacement of a precursor carbonate mineral (calcite, aragonite) within the brine-filled pores at the bottom of a hypersaline lake (Smith, 1979; Eugster and Smith, 1965; Smith et al., 1983; Olson and Lowenstein, 2021).

Peloidal Dolomite Grainstone

Description: Peloidal dolomite grainstone is composed of sand- and silt-sized peloidal grains of dolomitic mud (Figure 10a,b,c). Euhedral dolomite overgrowths occur on some peloid nuclei (Figure 10c). Thin beds are wavy and discontinuous, and, in some cases, small-scale cross-lamination was observed (Figure 10a,b).

Interpretation: Small-scale cross lamination is indicative of current or wave-reworking (Figure 10a,b). Rarely, these cross-stratified layers are symmetrical in cross section with oppositely dipping foresets, suggesting they were reworked by waves at or above wave base (Smoot, 1983). Northupite cements suggest the syndepositional occurrence of hypersaline brines, as discussed in the following section.

Diagenetic Saline Mineral Overprints

Shortite

Description: Shortite is abundant in dolomitic silty mudstone and oil shale in the WPM of the Solvay S-34-1 core as: 1) pseudomorphs after displacive crystals of gaylussite and pirssonite, 2) displacive crystalline aggregates, and 3) vein and fracture fills (Jagniecki and Lowenstein, 2015).

Euhedral displacive crystals (now single crystals and crystal aggregates of shortite) that appear triangular in cross section (1-5 mm) are common in oil shale and dolomitic silty mudstone (Figure 11a). These crystals exhibit monoclinic morphology (all three crystal axes are unequal in length, and two axes are perpendicular to one another), with a flattened wedge shape (Figure 11a). Surrounding sediment is compacted around the crystals, suggesting displacive growth before lithification. These crystals are now composed of shortite (orthorhombic), suggesting shortite has pseudomorphously replaced a monoclinic precursor mineral. Based on crystal morphology and modern analogues, the precursor mineral was probably gaylussite (monoclinic) (Olson and Lowenstein, 2021) (Figure 11a).

Displacive crystal aggregates of shortite are composed of crystals 0.5-2 mm in size. Displacive crystal aggregates typically contain pyrite and inclusions of the host sediment. Such shortite crystal aggregates crosscut laminae or surrounding layers are compacted around them (Figure 11b). The compaction of surrounding layers indicates formation before lithification.

Shortite, composed of interlocking crystalline mosaics, fills veins and fractures in oil shale and dolomitic silty mudstone (Figure 11c). Such shortite-filled horizontal and vertical fractures crosscut sedimentary laminae. Surrounding sediment is commonly compacted around the shortite.

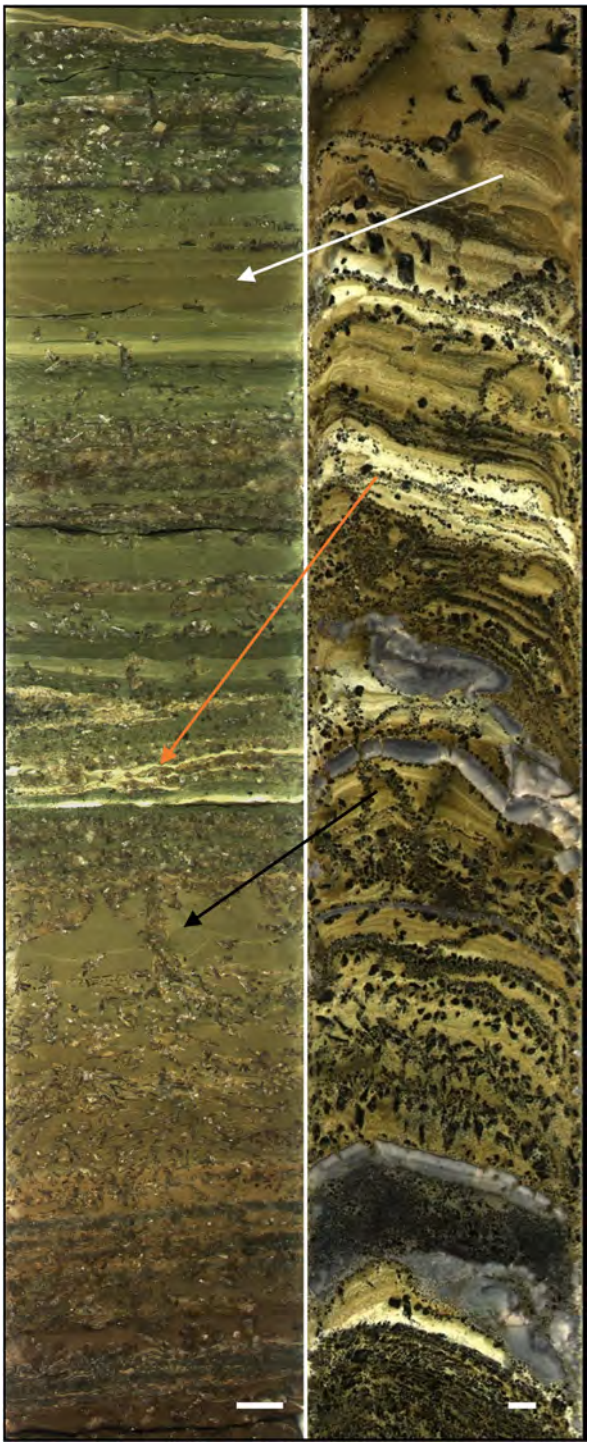

Figure 9. *Core photograph of GRCO-GRF16-1A-219Q-3-W (left) (~566.91-567.53 mbs) compared to Searles Lake SLAPP-SRLS17-1A-37V-1-A (right) (58.38-59.85 mbs). Laminated mud in the SLAPP core, deposited in a perennial saline lake, is similar in appearance to laminated silty dolomitic mudstone in the GRCO core (white arrow). Carbonate-rich laminae occur in the SLAPP (aragonite) and GRCO (dolomite) cores (red arrow). Diagenetic gaylussite crystals in the SLAPP core are similar in texture to shortite crystals in the GRCO core (black arrow). Laminated mud in the SLAPP core was bowed down on the edges during coring. Scale bar = 1 cm for both images.*

Interpretation: Pleistocene muds from Searles Lake contain euhedral gaylussite crystals that exhibit the same flattened wedge shape and monoclinic crystal structure as the crystal pseudomorphs in the Solvay core (Figure 11a) (Olson and Lowenstein, 2021). Experimentally, gaylussite and pirssonite dehydrate at elevated temperatures to form shortite (Bury and Redd, 1933; Jagniecki et al., 2013; Jagniecki and Lowenstein, 2015). Bury and Redd (1933) showed that at temperatures >40 °C gaylussite dehydrates to pirssonite. Jagniecki et al. (2013) showed that at temperatures >52 °C pirssonite dehydrates to shortite. Such processes probably led to pseudomorphous replacement by shortite in WPM sediments during burial (Jagniecki et al., 2013; Jagniecki and Lowenstein, 2015).

Northupite

Description: Northupite nodules, nodular aggregates, and cements occur in oil shale, dolomitic silty mudstone, and peloidal dolomite grainstone (Figure 11d, e). Northupite nodules are 1-3 mm in diameter and composed of dense crystal mosaics (Figure 11d). Northupite cement fills pore spaces in peloidal dolomite grainstones as large, poikilotopic crystals (Figure 11ei, eii). Peloids show no sign of compaction and cross stratification structures are well preserved.

Interpretation: Poikilotopic northupite cement filling voids in open frameworks of uncompacted dolomite peloids indicates that northupite formed during early, pre-compaction diagenesis. On the other hand, the lack of compaction around northupite nodules suggests they grew after lithification. Orientation of the nodules in mudstone is random, with no directional growth pattern. These features indicate a post-lithification, diagenetic origin.

Trona

Description: Diagenetic trona occurs in oil shale and dolomitic silty mudstone as displacive rosettes, 2-5 cm in diameter (Figure 11f). These rosettes commonly contain inclusions of detrital mud and pyrite (Figure 11f). Diagenetic trona rosettes also occur in cumulate trona layers of the evaporite subfacies (Figure 11g). Diagenetic trona crystals in mudstones and trona layers are randomly oriented and typically crosscut deformed mudstone or evaporite laminae (Figure 11f, g). Trona crystals ~ 200 µm to 5 mm in length also occur as a pseudomorphous replacement of bottom growth halite (Figure 5).

Interpretation: Mudstone and evaporite beds that surround trona rosettes commonly exhibit soft sediment deformation suggesting the trona rosettes formed before significant lithification occurred. Bottom-growth halite crystals replaced by trona were in-

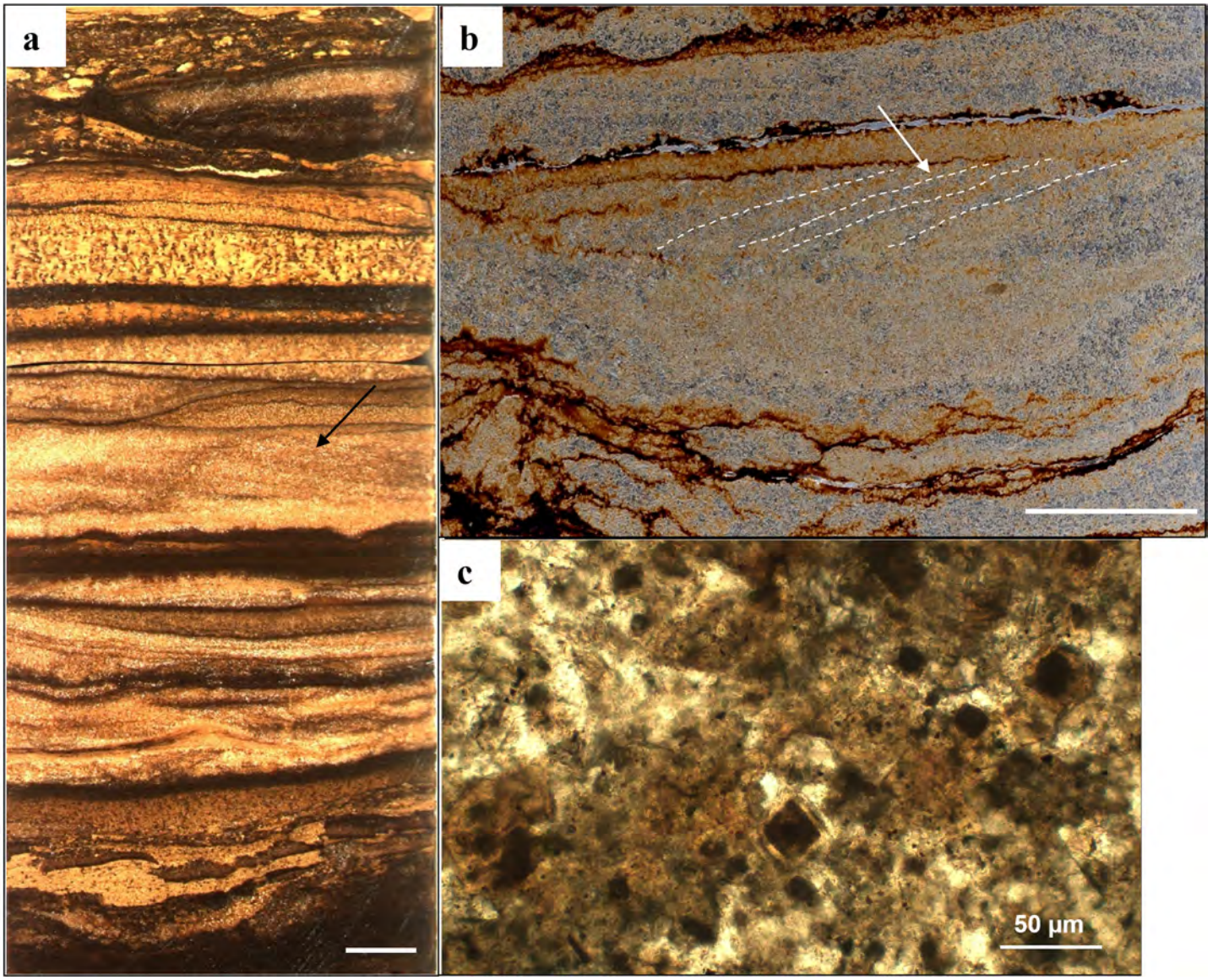

Figure 10. *Core photograph of a) wavy-bedded and cross-stratified (black arrow) dolomite peloids in peloidal dolomite grainstone. GRCO-GRF16-1A-210Q-4-W (540.25-540.85 mbs). Thin section photograph of b) cross-stratified dolomite peloid laminae (white arrow/dashed lines). GRCO-GRF16-1A-209Q-3 15-19 cm (536.69-537.30 mbs). Photomicrograph of c) dolomite mud peloids, some with dolomite overgrowths. GRCO-GRF16-1A-210Q-4 5-9 cm (540.23-540.86 mbs). Scale bar = 1 cm for a and b.*

terpreted by Jagniecki and Lowenstein (2015) to result from temperature increases during burial. To test this hypothesis, Jagniecki and Lowenstein (2015) modeled Na-carbonate-bicarbonate-rich brines from Lake Magadi, Kenya. They concluded that when brine temperature was raised during burial, halite partially dissolved, reintroducing Na back into the brine. Sodium derived from halite dissolution then caused supersaturation with respect to trona which precipitated in the void spaces left from dissolved halite, producing pseudomorphs.

Halite

Diagenetic halite occurs in the WPM as clear, fibrous satin-spar in vertical and horizontal fractures in silty dolomitic mudstone (Figure 11h). Fracture-fill halite is interpreted to have formed during movement of halite-saturated brines through hydraulic fractures (Birnbaum and Radlick, 1982; Leigh, 1991).

Alluvial Facies

The alluvial facies in the Solvay S-34-1 core consists of (1) massive mudstone, and (2) siliciclastic sandstone that together comprise alluvial marker beds A-I (Culbertson, 1961). Siliciclastic marker units in marginal localities of the Bridger subbasin are composed of trough cross-stratified sandstone, planar- to ripple-laminated sandstone, and climbing ripple cross-stratified sandstone. Pebble-sized rip-up clasts of sandstone and mudstone are common in the Bridger subbasin but rare in the Solvay core. These siliciclas-

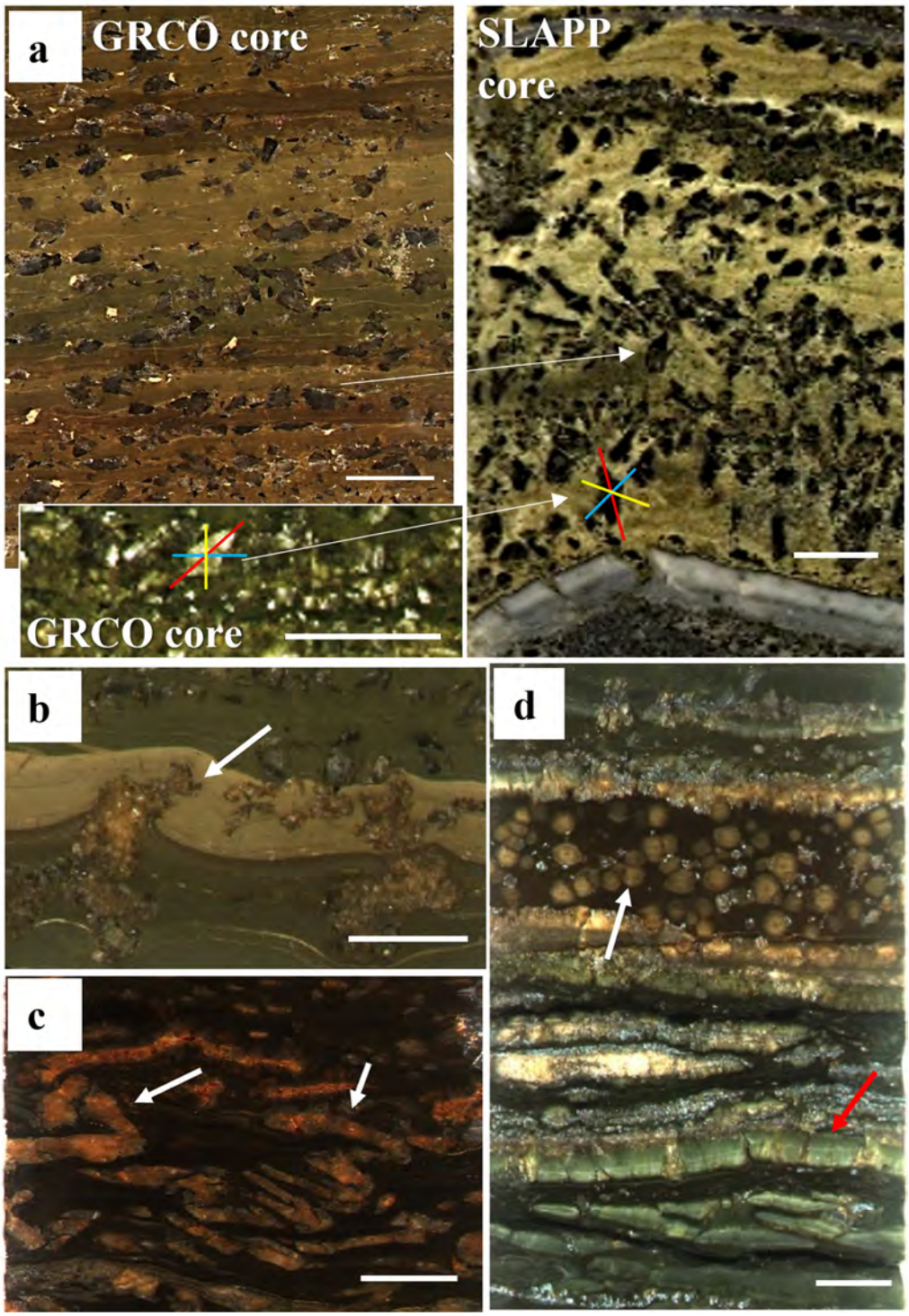

Figure 11. *Core photographs of diagenetic saline minerals:* ***a)*** *White arrows show gaylussite crystals in SLAPP core that have same morphology as shortite pseudomorphs after displacive gaylussite in GRCO core. Similarities include euhedral crystal terminations and flattened wedge shapes. Colored lines indicate crystal axes: red: a; blue: b; yellow: c. All lengths different. B and c axes are perpendicular to each other. Core photographs of: (left top) GRCO-GRF16-1A-170Q-6-W (422.45-422.80 mbs), (left bottom) GRCO-GRF16-1A-219Q-3-W (566.91-567.52 mbs), and (right) SLAPP-SRLS17-1A-37V-1-A (59.38-59.85 mbs).* ***b)*** *Shortite displacive crystal aggregate (white arrow) in silty dolomitic mudstone. Sediment is compacted around the shortite. GRCO-GRF16-1A-218Q-1-W (562.96-563.52 mbs).* ***c)*** *Fracture fill shortite in oil shale (white arrows). GRCO-GRF16-1A-223Q-5-W (584.31-584.71 mbs).* ***d)*** *Northupite nodules preferentially formed in mud laminae (white arrow). Dense northupite nodule mosaics completely replaced mud laminae (red arrow). GRCO-GRF16-1A-222Q-3-W (576.37-576.97 mbs).*

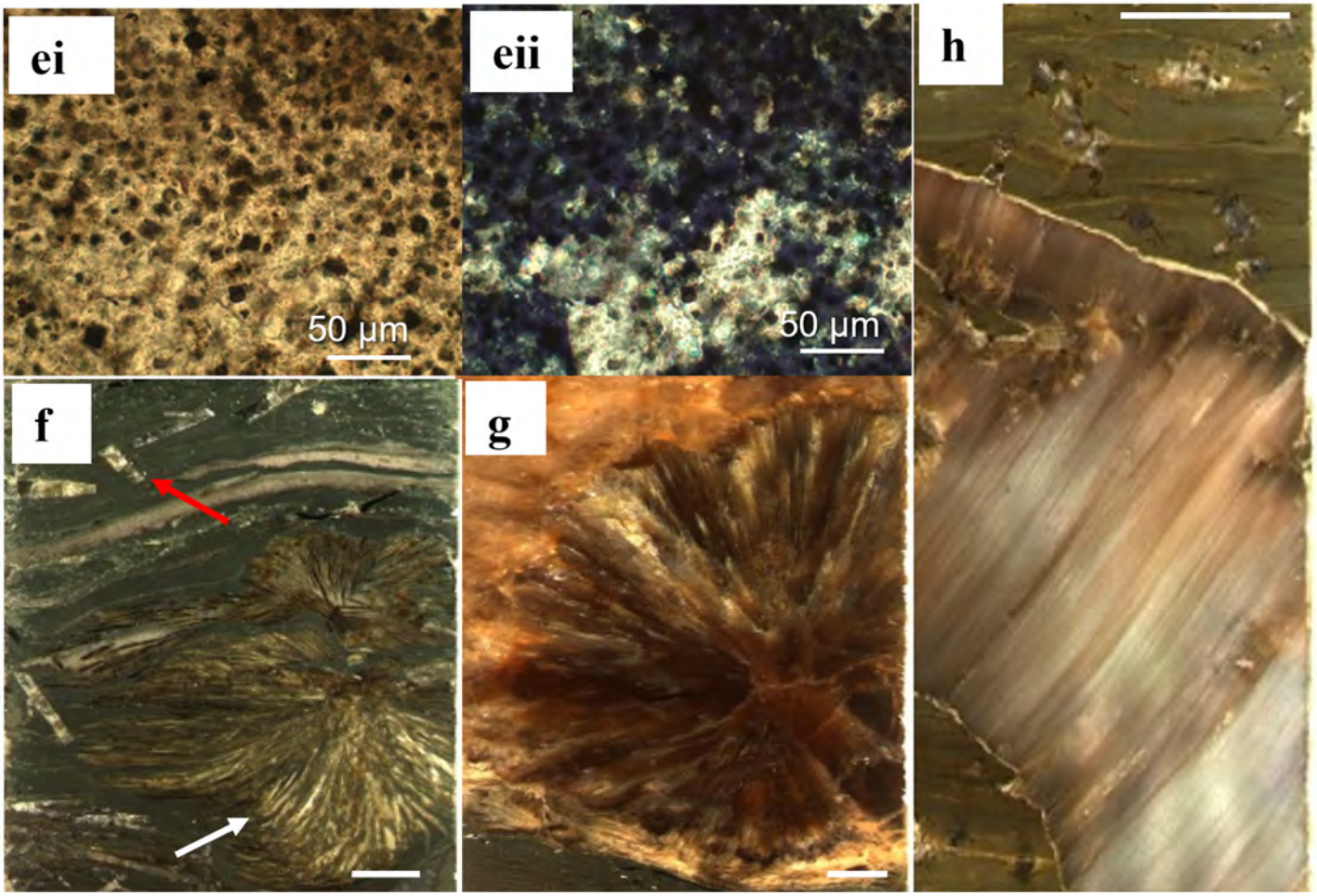

Figure 11 continued. *Core photographs of diagenetic saline minerals:* ***ei, eii)*** *Thin section photomicrograph of dolomite peloids cemented by northupite. Fig. ei was taken in plane polarized light; Fig. eii is viewed in cross-polarized light. Large interlocking crystals of northupite cement appear birefringent under cross-polarized light (Fig. eii). GRCO -GRF16-1A-210Q-4 5-9 cm (540.25-540.85 mbs).* ***f)*** *Trona rosette (white arrow) and randomly oriented needles in silty dolomitic mudstone. Randomly oriented tabular crystals (red arrow) are shortite. GRCO-GRF16-1A-234Q-6-W (614.65 -614.78 mbs).* ***g)*** *Trona rosette in bedded trona. GRCO-GRF16-1A-232Q-4-W (607.09-607.62 mbs).* ***h)*** *Halite "spar" filling fracture in mudstone. GRCO-GRF16-1A-234Q-2-W (612.26-612.85 mbs). Scale = 1 cm on all figures a-d and f-h.*

tic beds contain sandstone beds which alternate with faintly bedded to structureless mudstone and poorly developed paleosols (Eugster and Hardie, 1975; Smoot, 1983; Pietras and Carroll, 2006; Smith et al., 2015). Previous workers interpreted the marker units to have been deposited in fluvial, overbank, and shallow deltaic depositional environments.

Massive Mudstone Subfacies

Description: Siliciclastic marker units A-I in the Solvay S-34-1 core, from near the hydrologic low point of the Bridger subbasin, occur primarily as structureless to faintly laminated green mudstone (Figure 12a-d). Green mudstones, 2-20 m thick, contain Fe-bearing sulfides and oxides (pyrrhotite, pyrite, and magnetite), multiple generations of mud cracks, and other disruption features (Figure 12a,b).

Interpretation: Sediments of the basin-center marker beds are probably sheet delta deposits formed when sheet flood or fluvial channels intersected the margins of a standing body of water (perennial or ephemeral; Smoot and Lowenstein, 1991). Sheet delta deposits are commonly composed of clay, silt, and sand that accumulated in lakes, mudflats, and channels during flooding events. Mudstone layers with multiple generations of mudcracks and other disruption features indicate repeated wetting and drying episodes (Smoot, 1983; Smoot and Lowenstein, 1991). The common mudcracks in the siliciclastic marker units of the Solvay core establish desiccation near the hydrologic low point.

Siliciclastic Sandstone Subfacies

Description: Fine- to medium-grained siltstone and sandstone beds (1 cm to 0.5 m thick) contain abundant unidirectional cross-lamination and climbing ripple cross-stratification (Figure 12b,c).

Interpretation: Siliciclastic sandstones in marker

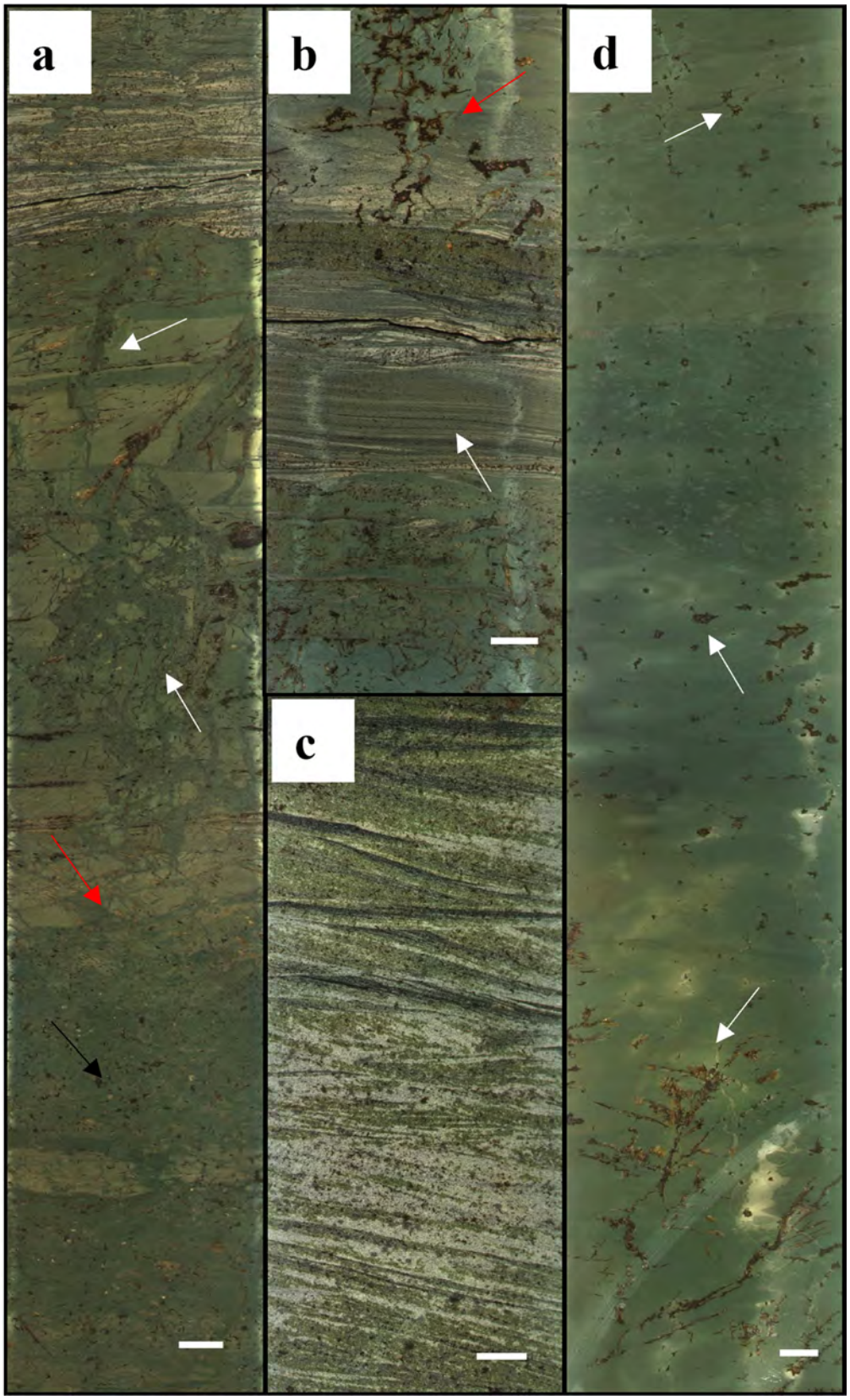

Figure 12. *Core photograph of: a) Disrupted mudstone and mudcracks (white arrows), proto-paleosol (red arrow) and sulfides (black arrow) in massive mudstone. GRCO-GRF16-1A-208Q-1-W (532.48-533.05 mbs). b) Silty laminated mudstone (white arrow) with mudcracks (red arrow). GRCO-GRF16-1A-208Q-3-W (533.68-534.30 mbs). c) Fine grained siliciclastic sandstone with small-scale cross stratification. GRCO-GRF16-1A-208Q-5-W (534.93-335.51 mbs). d) Massive mudstone with sulfides and organic material (white arrows). GRCO-GRF16-1A-208Q-4-W (534.31-534.933 mbs). Scale = 1 cm on all figures.*

beds A-I suggest significant shallowing or complete desiccation of Lake Gosiute, which allowed fluvial channel and sheet flood deposits to reach the basin center (Figure 12a-c) (Smoot, 1983; Smoot and Lowenstein, 1991).

WILKINS PEAK MEMBER LAKE EXPANSION-CONTRACTION SUCCESSIONS

Meter-scale vertical successions in the WPM were divided by Eugster and Hardie (1975) into four types defined by stratigraphic variations of five lithologies observed in outcrops (flat pebble conglomerate, oil shale, mudstone, lime sandstone and trona). Smoot (1983) described WPM vertical successions using seven dolomitic facies and evaporite. Smoot (1983) interpreted coarse grained sandstone and evaporite as shallow, marginal lake deposits, whereas carbonate mudstone and oil shales formed in deeper lakes. Pietras and Carroll (2006) and Smith et al. (2015) described WPM basin expansion-contraction successions beginning with transgressive intraclast conglomerate and calcareous sandstone deposits at the base, followed by deep-lake oil shale and detrital carbonate, capped with disrupted mudstone, siltstone, and evaporite.

Although the WPM facies successions are well recognized and documented, less work has been done detailing their evaporitic component. The evaporites of the Solvay S-34-1 core exhibit sedimentary structures which suggest they were predominantly deposited in perennial, anoxic, hypersaline lakes, and not on desiccated salt pans as hypothesized by previous authors (Eugster and Hardie, 1975; Smoot, 1983; Pietras and Carroll, 2006; Smith et al., 2015).

WPM vertical successions observed in the Solvay core are here defined by: (1) oil shale with or without (2) evaporite (perennial hypersaline lake), (3) peloidal dolomite grainstone and/or silty dolomitic mudstone (shallow saline lake, above wave base), and (4) massive mudstone with disruption features or desiccation cracks, and/or siliciclastic sandstone with ripple cross-stratification (subaerially-exposed mudflat-sheet delta) (Figure 13). Vertical changes of these four rock types indicate changes in lake depth (shallowing or deepening). Here, we define vertical successions on the basis of "shallowing-upward" trends. Authigenic dolomite mudstone is associated with oil shale and silty dolomitic mudstone, but, because of its rarity, was not included in this discussion of vertical successions.

An idealized shallowing-upward vertical succession observed in the Solvay S-34-1 core is illustrated in Figure 13. Oil shale, deposited during the deepest lake stage, occurs at the base of the succession. This interpretation is supported by the wide lateral extent of many oil shales (Smith et al., 2015), the complete lack of evidence for exposure or shallow-water features in oil shales, and their high organic matter content and Fe-sulfide minerals, which suggests prolonged lake anoxia.

In the idealized shallowing-upward succession, oil shale (deepest lake stage) is overlain by and commonly interlayered with bedded evaporite. Fine scale interlaying of oil shale and evaporite (Figure 4a) suggests that oil shales were deposited in saline waters, but below trona saturation. Bedded evaporite indicates lake shallowing and salinity increase to reach saturation with respect to trona and halite while maintaining continuous subaqueous conditions. Well-preserved evaporites in the Solvay core, with only rare evidence for syndepositional dissolution, suggests evaporite deposition occurred below the thermocline in a density stratified lake, such as in the modern Dead Sea where the thermocline occurs at depths of 20-30 m (Sirota et al., 2017).

Observations from the modern Dead Sea suggest that cumulate trona was deposited during the colder, winter months, whereas bottom growth evaporites were formed during the warmer, summer months (Sirota et al., 2017). Rare occurrences of bottom growth trona with dissolution surfaces, like those observed in trona from Lake Magadi, Kenya, probably represent periods when the lake shallowed (McNulty et al., 2017). The WPM oil shale and evaporite deposits in the Solvay core are similar to those found in modern Mono Lake and Lake Bogoria, Kenya, where deposition of organic matter-rich muds and evaporites is common (Domagalski et al.,1989; Renaut et al., 2013; Jagniecki and Lowenstein, 2015; Lowenstein et al., 2017).

In the idealized shallowing upward succession, oil shale and evaporite are overlain by peloidal dolomitic grainstone or silty dolomitic mudstone. The important characteristics of these two subfacies are wave ripples, which indicate reworking by waves at or above wave base, and coarser sediment, suggesting deposition in shallower water or closer to the shoreline than where oil shale was deposited. Mud peloids, for example, occur along the shoreline of the modern Dead Sea in waters shallower than wave base (Lowenstein et al., 2021). Shortite after gaylussite, and northupite nodules and cement in silty dolomitic mudstone and peloidal dolomitic grainstone, suggest saline, $Na\text{-}CO_3\text{-}HCO_3$-rich brines existed at the time of deposition of peloidal dolomitic grainstone and silty dolomitic mudstone (Smith, 1979; Eugster and Smith, 1965; Olson and Lowenstein, 2021).

In the idealized shallowing-upward succession,

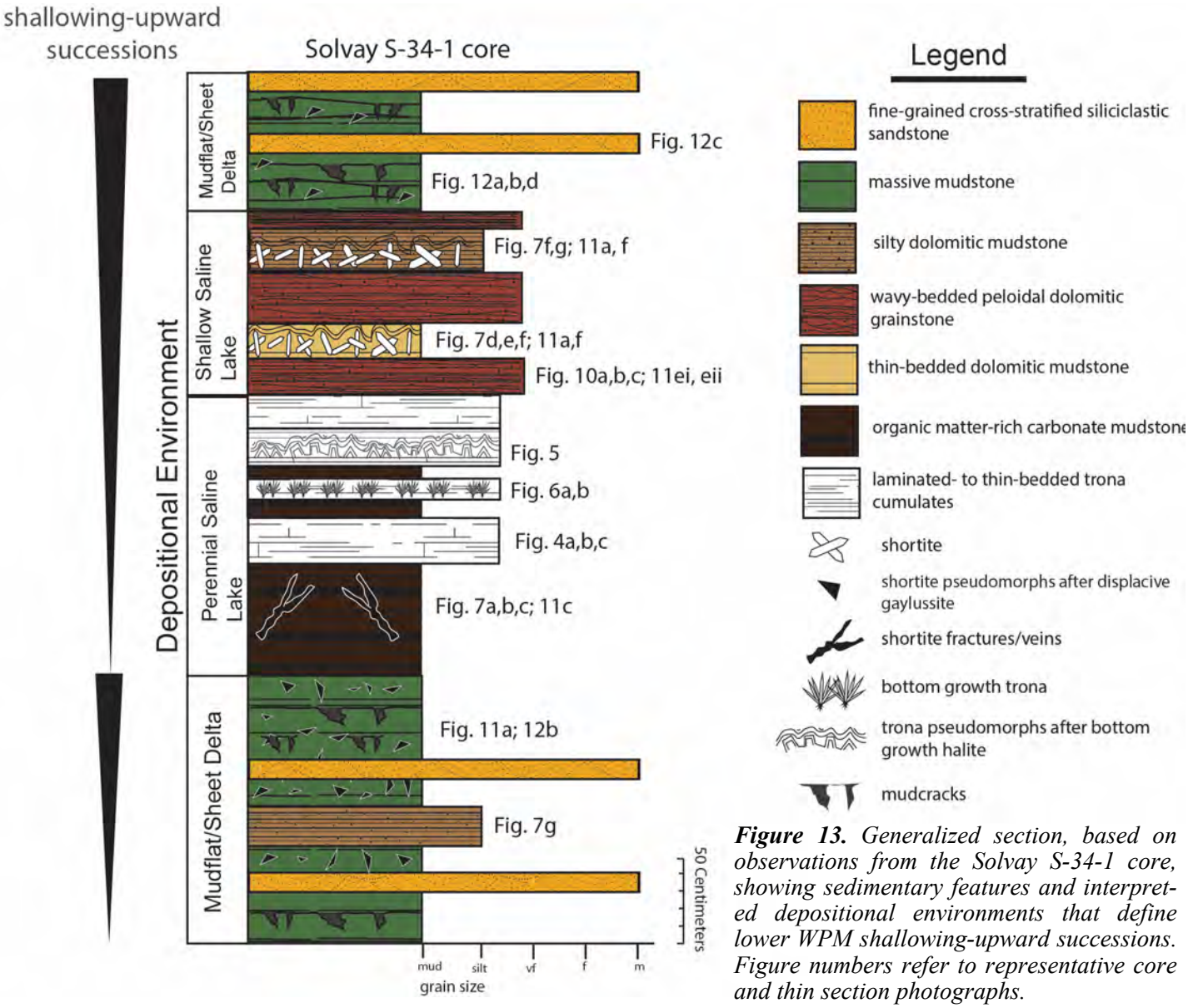

Figure 13. *Generalized section, based on observations from the Solvay S-34-1 core, showing sedimentary features and interpreted depositional environments that define lower WPM shallowing-upward successions. Figure numbers refer to representative core and thin section photographs.*

peloidal dolomitic grainstone or silty dolomitic mudstone are overlain by massive mudstone with mudcracks and paleosol features and/or siliciclastic sandstone with ripple cross-stratification of marker beds A -I. Mudcracks and paleosol features indicate desiccation. Siliciclastic sandstones also suggest significant shallowing or desiccation of the lake, allowing for deposition of channel and sheet flood deposits (Smoot, 1983; Smoot and Lowenstein, 1991). In the Solvay core, mudcracked mudstones become common in the WPM above Trona Bed 16, which marks the northward shift of the Bridger subbasin depocenter (Walters et al., in review). Such a northward depocenter shift, and the lack of evaporites above the lower WPM in the Solvay core, indicate that trona deposition migrated to a more northward area of the Bridger subbasin. Despite this shift of the depocenter, oil shale layers occur in the Solvay core throughout the WPM, which shows that large lakes existed in Lake Gosiute throughout WPM deposition.

Defined as above, there are 48 shallowing upward successions in the WPM of the Solvay S-34-1 core (Figure 14). Eighteen of these successions contain unequivocal evidence (mudcracks) for a perennial saline lake shallowing and drying out. The remaining 30 shallowing-upward successions exhibit evidence of lake shallowing, but not desiccation. For example, at 585 m and above, oil shale and Trona Bed 9 (TB9) (perennial saline lake: deepest lake), are overlain by peloidal dolomite grainstone and silty dolomitic mudstone (saline lake, shallower than wave base). Oil shale and evaporite from TB10 (perennial saline lake: deepest lake water depth) lie above the peloidal dolomite grainstone and silty dolomitic mudstone. This succession lacks massive mudstone or siliciclastic sandstone or any evidence of basin desiccation. But the vertical transition from oil shale to evaporite to peloidal dolomite grainstone and silty dolomitic mudstone (one shallowing upward succession) and then back to oil shale and evaporite (base of overlying

Figure 14. *Detailed measured section of Wilkins Peak Member interval in the Solvay S-34-1 core. Black triangles show 48 shallowing-upward successions.*

shallowing upward succession) implies lake shallowing followed by deepening. Of the 18 shallowing-upward successions below Trona Bed 16 and the shift in the basin depocenter, only four contain evidence for complete desiccation at the hydrologic low point. Above Trona Bed 16 and the northward shift of the basin depocenter, basin desiccation is much more common (14 out of 30 successions contain mudcracks).

CONCLUSIONS

1. The close association of oil shale with bottom growth evaporite and cumulate trona in the WPM in the Solvay S-34-1 core indicates evaporite accumulation below the thermocline of a perennial hypersaline lake and not a saline pan as interpreted by previous workers.

2. Interlayered trona and oil shale represent periods when lake waters were above and below trona saturation, likely due to seasonal temperature changes of the hypersaline brine body.

3. Rare instances of trona with dissolution surfaces represent periods of evaporite accumulation in a shallower saline lake with no thermocline, similar to Lake Magadi, Kenya where bottom growth trona with dissolution surfaces is common.

4. Mudcracked mudstones and siliciclastic sandstones in the WPM of the Solvay core represent periodic desiccation at the hydrologic low point of the Bridger subbasin. After deposition of Trona Bed 16, the basin depocenter shifted northward, and the abundance of mudcracked mudstone associated with alluvial marker bed facies increases, and evaporites are rare.

5. Dolomitic mudstone laminae are commonly compacted around diagenetic shortite crystals (commonly as pseudomorphs after gaylussite), suggesting displacive growth before lithification. This implies that Na-CO_3-HCO_3-rich brines existed during deposition and burial temperatures reached at least 52°C.

6. Four key facies indicators used to define repetitive shallowing upward successions in the Solvay core are (1) oil shale with or without (2) evaporite (perennial hypersaline lake), (3) peloidal dolomitic grainstone and/or silty dolomitic mudstone (shallow saline lake, above wave base) and (4) massive mudstone with disruption features or desiccation cracks, and/or siliciclastic sandstone with ripple cross-stratification (mudflat-sheet delta).

7. In the Solvay core, there are 48 shallowing-upward successions, 18 of which contain key lithologies diagnostic of lake desiccation. Of the 18 shallowing-upward successions deposited near the hydrologic low point (successions below Trona Bed 16), 4 show evidence for complete desiccation.

ACKNOWLEDGMENTS

We thank the National Science Foundation Integrated Earth Systems Program to University of Wisconsin, (NSF-EAR 1813278), Binghamton University (NSF-EAR 1812741), and Northern Arizona University (NSF-EAR 1813350), the American Association of Petroleum Geologists, the Geological Society of America, and LacCore National Lacustrine Core Facility for providing support for this project. We thank Solvay Minerals Co. for donating the Solvay S-34-1 core for this work. We gratefully acknowledge the staff at LacCore, University of Minnesota: Kristina Brady Shannon, Anders Noren, Ryan O'Grady, Amy Myrbo, Mark Shapley, Alex Stone and Jessica Heck for their help storing and processing the Solvay core. We acknowledge the Solvay core processing party including Andrew Walters, Shlomo Honig, and Isaac Sageman. We acknowledge and thank Binghamton Master's thesis committee member Robert Demicco and Kevin Bohacs of KMBohacs GEOconsulting for their reviews. Finally, we thank Elliot Jagniecki and Mike Vanden Berg of the Utah Geological Survey for encouraging publication of this work.

REFERENCES

Aswasereelert W, Meyers SR, Carroll AR, Peters SE, Smith ME, Feigl KL (2013) Basin-scale cyclostratigraphy of the Green River Formation, Wyoming. Geological Society of America Bull. 125:216-228

Birnbaum SJ, Radlick TM (1982) Depositional and Diagenetic Spectra Of Evaporites: A Core Workshop, Calgary, Canada, June 26-27, 1982. Department of Environmental Science and Geology, Wayne State University Detroit, Michigan 48202 3:75

Bohacs KM (1998) Contrasting Expressions of Depositional Sequences in Mudrocks from Marine to Non Marine Environments. Mudstones and Shales, vol. 1, Characteristics at the basin scale: Stuttgart p. 32-77

Boni PL, Atkinson WW (1998) A mineralogic and stratigraphic profile of trona bed 17 in the Solvay trona mine near Green River, Wyoming. Proceedings of the First International Soda Ash Conference, Public Information Circular No. 40, pp. 21-32

Bradley WH (1962) Chloroplast in Spirogyra from the Green River Formation of Wyoming. American Journal of Science 260:455-459

Bradley WH, Eugster HP (1969) Geochemistry and Paleolimnology of the Trona Deposits and Associated Authigenic Minerals of the Green River Formation of Wyoming. U.S. Geological Survey Professional Paper 496-B:B1-71

Bury CR, Redd R (1933) The System Sodium Carbonate-Calcium Carbonate-Water. Journal of Chemical Society, London, 272:1160-1162

Carroll AR, Bohacs KM (2001) Lake-Type Control on Petroleum Source Rock Potential in Nonmarine Basins. American Association of Petroleum Geologists Bull 85:1033-1053

Culbertson WC (1961) Stratigraphy of the Wilkins Peak Member of the Green River Formation, Firehole Basin Quadrangle, Wyoming. U.S. Geological Survey Professional Paper 424D: 170-173

Culbertson WC (1962) Laney Shale Member and Tower Sandstone Lentil of the Green River Formation, Green River area, Wyoming, IN Geological Survey research 1962; short papers in geology, hydrology, and topography; Articles 60-119: U.S. Geological Survey Professional Paper, 450-C, p. C54-C57

Culbertson WC (1966) Trona in the Wilkins Peak Member of the Green River Formation, Southwestern Wyoming. U.S. Geological Survey Professional Paper 550-B:B159-B164

Culbertson WC (1971) Stratigraphy of the trona deposits in the Green River Formation, Southwest Wyoming. Rocky Mountain Geology 10:15-23

Demicco RV and Lowenstein TK (2020) When "evaporites" are not formed by evaporation: The role of tem-perature and pCO_2 on saline deposits of the Eocene Green River Formation, Colorado, USA: Geological Society of America Bulletin, 132:1365–1380

Domagalski JL, Orem WH, Eugster HP (1989) Organic geochemistry and brine composition in Great Salt, Mono, and Walker Lakes. Geochim.Cosmochim. Acta 53:2857-2872

Dyni JR (1996) Sodium Carbonate Resources of The Green River Formation in Utah, Colorado, and Wyoming. US Geological Survey open-file report, 96–729:42

Dyni JR (1998) Sodium Carbonate Resources of the Green River Formation. U.S. Geological Survey open-file report, pp 37-47

Dyni, JR, Hawkins JE (1981) Lacustrine turbidites in the Green River Formation, northwestern Colorado. Geology 9, 235-238

Eugster HP, Hardie LA (1975) Sedimentation in an Ancient Playa-Lake Complex: The Wilkins Peak Member of The Green River Formation of Wyoming: Geological Society of America, Bulletin 86:319–334

Eugster HP, Smith GI (1965) Mineral Equilibria in the Searles Lake Evaporite, California. Journal of Petrology, 6:473-522

Fahey JJ (1962) Saline Minerals of the Green River Formation, with a Section on X-ray Powder Data for Saline Minerals of the Green River Formation by M.E. Mrose. U.S. Geological Survey Professional Paper 405:50

Fischer AG, Roberts LT (1991) Cyclicity in the Green River Formation (lacustrine Eocene) of Wyoming: Journal of Sedimentary Petrology, 61:1146 –1154

Jagniecki EA, Jenkins DM, Lowenstein TK, Carroll AR (2013) Experimental Study of Shortite ($Na_2Ca_2(CO_3)_3$) Formation and Application to the Burial History of the Wilkins Peak Member, Green River Basin, Wyoming, USA. Geochimica et Cosmochimica Acta, 115:31-45

Jagniecki EA, Lowenstein TK (2015) Evaporite of the Green River Formation, Bridger and Piceance Creek Basins; Deposition, Diagenesis, Paleobrine Chemistry, and Eocene Atmospheric CO_2. M.E. Smith, A.R. Carroll (eds.), Stratigraphy and Paleolimnology of the Green River Formation, 77-309

Johnson RC, Mercier TJ, Brownfield ME, Pantea MP, Self JG (2010) An assessment of in-place oil shale resources in the Green River Formation, Piceance Basin, Colorado. US Geol Surv Digital Data Series, DDS-69-Y:187

Leigh RT (1991) Wyoming Trona: An Overview of the Geology and Economic Utilization. Wyoming Association Guidebook, 42nd field conference103-120

Lowenstein TK, Hardie LA (1985) Criteria for the recognition of salt-pan evaporites. Sedimentology, 32(5):627-644

Lowenstein TK, Li J, Brown C, Roberts SM, Ku TL, Luo S, Yang W (1999) 200 ky paleoclimate record from Death Valley salt core. Geology, 27(1):3-6

Lowenstein TK, Jagniecki EA, Carroll AR, Smith ME, Renaut R, Owen R (2017) The Green River salt mystery: What was the source of the hyperalkaline lake waters? Earth-Science Reviews, 173:295-306

McNulty EP, (2017) Lake Magadi and the Soda Lake Cycle: A Study of the Modern Sodium Carbonates and of Late Pleistocene and Holocene Lacustrine Core Sediments. Master's Thesis, Binghamton University

Meyers SR, Sageman BB, Pagani M (2008) Resolving Milankovitch: Consideration of Signal and Noise. American Journal of Science, 308:770-786

Murphy JT, Lowenstein TK, Pietras JT (2014) Preservation of Primary Lake Signatures in Alkaline Earth Carbonates of The Eocene Green River Wil-

kins Peak-Laney Member Transition Zone. Sedimentary Geology, 314:75–91

Olson KJ, and Lowenstein TK (2021) Searles Lake evaporite sequences: Indicators of Late Pleistocene/Holocene lake temperatures, brine evolution, and pCO_2. Geological Society of America Bulletin, 133: 2319-2334

Pietras JT, Carroll AR (2006) High-Resolution Stratigraphy of An Underfilled Lake Basin: Wilkins Peak Member, Eocene Green River Formation, Wyoming, U.S.A. Journal of Sedimentary Research, 76:1197–1214

Pietras JT, Carroll AR, Rhodes MK (2003) Lake Basin Response to Tectonic Drainage Diversion, Eocene Green River Formation, Wyoming: Journal of Paleolimnology, 30:115–125

Renaut RW, Owen RB, Jones B, Tiercelin J-J, Tartis C, Ego JK, Konhauser KO (2013) Impact of Lake-Level Changes on the Formation of Thermogene Travertine in Continental Rifts: Evidence from Lake Bogoria, Kenya Rift Valley. Sedimentology, 60:428-468

Robb WA, Smith JW (1976) Mineral Profile of Wyoming's Green River formation—Sampled by Blacks Fork Core. Wyoming Geological Association Earth Science Bulletin, 9:1-7

Roehler HW (1992) Description and correlation of Eocene rocks in stratigraphic reference sections for the Green River and Washakie basins, Southwest Wyoming. United States Geological Survey, Professional Paper, 1506

Scott JJ, Smith ME (2015). Trace Fossils of the Eocene Green River Lake Basins, Wyoming, Utah, and Colorado. Stratigraphy and Paleolimnology of the Green River Formation, Western USA. Springer, Dordrecht, 313-350

Sirota I, Enzel Y, Lensky NG (2017) Temperature seasonality control on modern halite layers in the Dead Sea: In situ observations. Geological Society of America Bulletin 129, 1181-1194

Smith, GI (1979) Subsurface stratigraphy and geochemistry of late Quaternary evaporites, Searles Lake, California. U.S. Geological Survey Professional Paper, 1043:130

Smith GI, Barczak J, Moulton GF, Liddicoat JC (1983) Core KM-3, a Surface-to-Bedrock Record of Lake Cenozoic Sedimentation in Searles Valley, California. U.S. Geologic Survey Professional Paper, 1256:24

Smith ME, Carroll AR, Singer BS (2008) Synoptic Reconstruction of a Major Ancient Lake System: Eocene Green River Formation, Western United States. Geological Society of America Bulletin, 120:54–84

Smith ME, Chamberlain KR, Singer BS, Carroll AR (2010) Eocene Clocks Agree: Coeval 40Ar/39Ar, U-Pb, And Astronomical Ages from The Green River Formation. Geology, 38:527–530

Smith ME, Carroll AR, Scott JJ, Singer BS (2014) Early Eocene carbon isotope excursions and landscape destabilization at eccentricity minima: Green River Formation of Wyoming. Earth and Planetary Science Letters, 403:393-406

Smith ME, Carroll AR, Scott JJ (2015) Stratigraphic Expression of Climate, Tectonism, and Geomorphic Forcing in an Underfilled Lake Basin: Wilkins Peak Member of the Green River Formation. M.E. Smith, A.R. Carroll (eds.), Stratigraphy and Paleolimnology of the Green River Formation, 277-309

Smoot JP (1983) Depositional Subenvironments in an Arid Closed Basin; Wilkins Peak Member of The Green River Formation (Eocene), Wyoming, U.S.A. Sedimentology, 30:801–827

Smoot JP, Lowenstein TK, (1991) Depositional Environments of Non-Marine Evaporites, In Melvin, J.L., Ed., Evaporite, Petroleum and Mineral Resources: New York, Elsevier, Developments in Sedimentology, 50:189–347

Tissot BP, Vandenbroucke M (1983) Geochemistry and Pyrolysis of Oil Shales. Mikins, F.P., McKay, J.F. (eds.), Geochemistry and Chemistry of Oil Shales, Washington, DC, American Chemical Society, Symposium Series, 230:1-11

Wiig SV, Grundy WD, Dyni JR (1979) Trona Resources in the Green River Basin, Southwest Wyoming. U.S. Geological Survey open-file report, 95-47